

Interplay between the Conformational Flexibility and Photoluminescent Properties of Mononuclear Pyridinophanecopper(I) Complexes

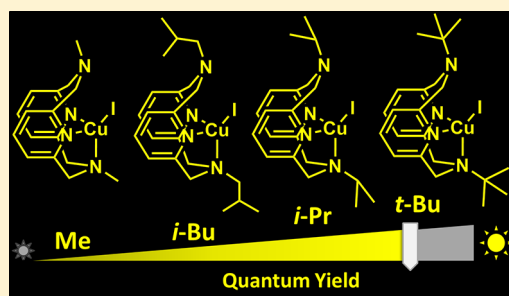
Pradnya H. Patil,[†] Georgy A. Filonenko,[†] Sébastien Lapointe,[†] Robert R. Fayzullin,[‡] and Julia R. Khusnutdinova^{*,†}

[†]Coordination Chemistry and Catalysis Unit, Okinawa Institute of Science and Technology Graduate University, 1919-1 Tancha, Onna-son, Kunigami-gun, Okinawa 904-0495, Japan

[‡]Arbuzov Institute of Organic and Physical Chemistry, Federal Research Center, Kazan Scientific Center, Russian Academy of Sciences, 8 Arbuzov Street, Kazan 420088, Russian Federation

Supporting Information

ABSTRACT: The macrocyclic ligand conformational behavior in solution, solid-state structures and the photophysical properties of copper(I) cationic and neutral mononuclear complexes supported by tetradentate *N,N'*-dialkyl-2,11-diaza[3.3](2,6)-pyridinophane ligands ^RN4 (R = H, Me, ⁱBu, ^{sec}Bu, ^{neo}Pent, ⁱPr, Ts) were investigated in detail. Steric properties of the alkyl group at the axial amine in the ^RN4 ligand were found to strongly affect the conformational preferences and dynamic behavior in solution. Several types of conformational exchange processes were revealed by variable-temperature NMR and 2D exchange spectroscopy, including degenerative exchange in a pseudotetrahedral species as well as exchange between two isomers with different conformers of tri- and tetracoordinate ^RN4 ligands. These exchange processes are slower for the complexes containing bulky alkyl groups at the amine compared to less sterically demanding analogues. A clear correlation is also observed between the steric bulk of the alkyl substituents and the photoluminescent properties of the derived complexes, with less dynamic complexes bearing bulkier alkyl substituents exhibiting higher absolute photoluminescence quantum yield (PLQY) in solution and the solid state: PLQY in solution increases in the order Me < ^{neo}Pent < ⁱBu < ^{sec}Bu ≈ ⁱPr < ^tBu. The electrochemical properties of the cationic complexes [(^RN4)Cu^I(MeCN)]X (X = BF₄, PF₆) were also dependent on the steric properties of the amine substituent.



INTRODUCTION

During the past decades, photoluminescent (PL) materials have been widely utilized as sensors, electroluminescent displays, and probes of biological systems.^{1–17} Among these materials, d⁶ and d⁸ transition-metal complexes such as iridium(III), ruthenium(II), osmium(II), rhenium(I), and platinum(II) are extensively used because of their stability, tunability, and high efficiencies.^{18–29} Another important class of PL compounds contains d¹⁰ coinage metals such as silver(I), gold(I), and copper(I).^{30–36} Among these compounds, copper(I) complexes are of considerable interest because of their low price and availability as an alternative to more expensive precious metal-based PL materials.^{32,37–39} Over the last several decades, a great variety of copper(I) PL complexes have been developed that include copper clusters, halide-bridged complexes, mono- and polynuclear phosphine complexes, homo- or heteroleptic species with diimine-type ligands, and recently developed N-heterocyclic carbene and amide complexes.^{40–52} A variety of strategies were developed to control the emissive properties of copper(I) complexes, mostly based on variation of the supporting ligand electronic properties^{42,53,54} or, in some cases, control of the configurational changes using the steric properties of the

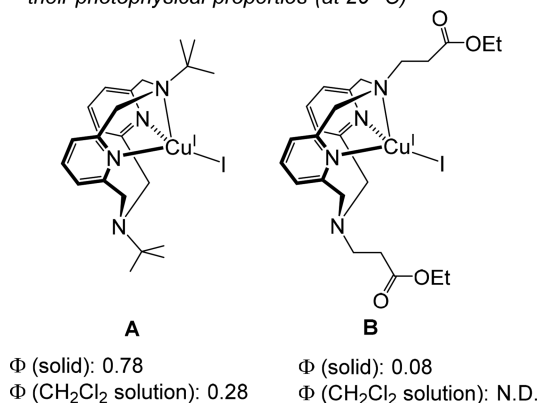
ligand.^{45,55,56} However, one of the common problems that can limit the practical application of copper(I) complexes is their lability in solution, leading to dissociation of polynuclear species or, in the case of heteroleptic mononuclear complexes, ligand dissociation and exchange.^{53,57–59}

We have recently reported a series of solution-stable, PL mononuclear copper(I) complexes supported by the tetradentate ligand *N,N'*-dialkyl-2,11-diaza[3.3](2,6)-pyridinophane (^RN4).⁶⁰ These N-donor ligands are synthetically easily accessible and allow for various structural modifications by varying the nature of the amine substituent, while macrocycle coordination to a Cu center leads to the formation of well-defined mononuclear complexes.⁶¹ In particular, complexes A and B (Scheme 1a) were found to be emissive in the solid state, with the absolute photoluminescence quantum yield (PLQY) reaching 0.78 for complex A but only 0.08 for complex B. Moreover, complex A also showed emission in a dichloromethane solution at 20 °C, while complex B was not emissive.

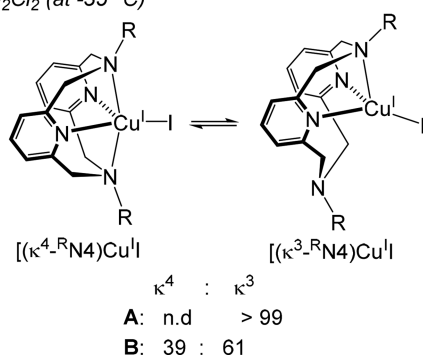
Received: April 30, 2018

Scheme 1. Previously Reported (^RN4)Cu^I Complexes⁶⁰

a) Previously reported (^RN4)Cu^I complexes and their photophysical properties (at 20 °C)



b) Conformational equilibria in solutions of **A** and **B** in CD₂Cl₂ (at -35 °C)



Another notable feature of these complexes was the conformational flexibility of the macrocyclic ligand in solution,^{62,63} leading to the formation of two isomeric complexes (Scheme 1b). In particular, we have reported that the cationic complexes [^RN4]Cu^I(MeCN)⁺ (MeCN = acetonitrile) and the neutral complexes **A** and **B** exist as two isomers in solution, in which the ^RN4 ligand binds to the Cu center with three N donors or with all four N donors coordinating in a κ^3 or κ^4 fashion, respectively.⁶⁰ A comparison of the solution behavior of **A** and **B** studied by NMR spectroscopy showed that the *tert*-butyl (^tBu)-substituted complex **A** exists only as a tetracoordinate species in solution with a κ^3 -bound ^tBuN4 ligand, while complex **B** exists in an equilibrium between two isomers with κ^3 - and κ^4 -bound ligands in a 61:39 ratio, respectively, at -35 °C. We hypothesized that this is due to the difference in steric bulk of the alkyl substituents

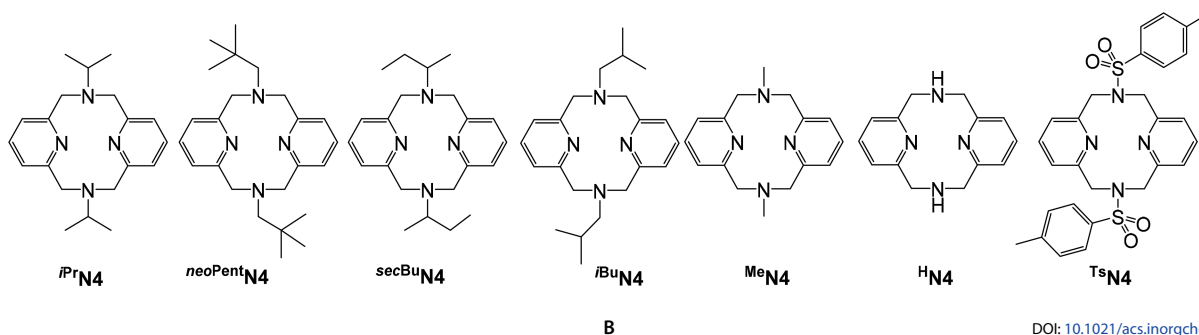
at the axial amine donor rather than their electronic properties. Moreover, the greater flexibility of complex **B** could contribute to the absence of emission in solution in contrast to the ^tBu-substituted complex **A**. However, the effect of the ester functional group in complex **B** could not be completely excluded because the length of the ester-containing substituent is sufficiently long to allow “wrapping around” the metal center, resulting in weak interaction of the metal with the ester functional group and “exciplex” quenching.^{38,51,64,65} Therefore, a comparison over a more diverse range of ligands is required to elucidate the role of structural factors in determining the photophysical properties of the derived complexes.

We recently reported that the ^RN4 ligand dynamic behavior in copper(I) complexes has an important implications in the development of mechanoresponsive polymer materials. We showed that the analogous ^RN4-based copper(I) complexes containing a bulky alkyl group at the amine can be covalently attached to the polyurethane linear chain, acting as a stress-responsive PL probe showing fast and reversible emission intensity changes in response to tensile stress in polyurethane films.⁶⁶ Further studies showed that this is likely due to suppression of the nonradiative decay pathway in samples subjected to stress, likely reflecting the dynamics within the macrocyclic ligand.⁶⁶

In order to better design mechanoresponsive materials, we decided to carry out a systematic study of the main factors that affect the photophysical properties of complexes similar to the ones used in the copper(I)-incorporated polyurethane study.

In the current work, we investigated in detail the solid-state structures, redox and photophysical properties, solution dynamic behavior, and conformational equilibria in a series of cationic and neutral copper(I) complexes supported by the tetradentate pyridinophane-type ligands. We assessed the steric effect of the amine substituents on the conformational preference and dynamics in the series of cationic [^RN4]Cu^I(MeCN)⁺ and neutral (^RN4)Cu^I complexes where R = hydrogen (H), methyl (Me), isobutyl (ⁱBu), *sec*-butyl (^{sec}Bu), *neo*-pentyl (^{neo}Pent), and isopropyl (ⁱPr) (Chart 1). In addition, the strength of the copper(I) interaction with axial amine donors was varied using electron-poor tosyl (Ts)-substituted complexes [(^{Ts}N4)Cu^I(MeCN)]⁺ and (^{Ts}N4)Cu^I (Chart 1). The comparison of these complexes demonstrates that the steric properties of the amine substituent are the main factors controlling the conformational preference and dynamics in solution as well as the photophysical properties of the derived complexes. 2D exchange spectroscopy (EXSY) and variable-temperature (VT) NMR spectroscopy studies also revealed several types of exchange processes involved in the conformational equilibria in solution. For both cationic and neutral complex series, increasing steric hindrance is associated with

Chart 1. Ligands Studied in This Work



greater preference for the tetracoordinate complexes in solution. Moreover, steric hindrance was found to affect the redox properties of the cationic complexes. The current study demonstrates that a synthetically simple modification of the axial amine steric properties leads to significant variation of the emissive properties. This can be used as a strategy to design solution-stable mononuclear copper(I) complexes with macrocyclic N-donor ligands, by contrast to many other transition-metal-based systems where synthetically demanding variation of the electronic properties of the surrounding ligands is needed.

EXPERIMENTAL DETAILS

General Specifications. All manipulations were carried out under an argon atmosphere using standard Schlenk and MBRAUN glovebox techniques if not indicated otherwise. All reagents for which the synthesis is not given were commercially available from Sigma-Aldrich, TCI, and Nacalai Tesque and were used as received without further purification. Anhydrous solvents were dispensed from an MBRAUN solvent purification system and degassed prior to use. Anhydrous deuterated solvents were purchased from Euriso-top and stored over 4 Å molecular sieves.

Ligands *N,N'*-diisopropyl-2,11-diaza[3,3](2,6)pyridinophane (^{Pr}N4),⁶⁷ *N,N'*-dimethyl-2,11-diaza[3,3](2,6)pyridinophane (^{Me}N4),⁶⁸ 2,11-diaza[3,3](2,6)pyridinophane (^HN4),⁶⁸ and *N,N'*-ditosyl-2,11-diaza[3,3](2,6)pyridinophane (^{Ts}N4)⁶⁸ were prepared according to the literature procedures. [Cu(MeCN)₄]⁺ precursors were prepared by dissolving Cu₂O in an MeCN solvent in the presence of aqueous HBF₄ or HPF₆, followed by two consecutive recrystallizations from cold MeCN.⁶⁹ NMR spectra were recorded on JEOL ECZ400S 400 MHz and ECZ600R 600 MHz spectrometers. Chemical shifts are referenced internally to the residual solvent signals. 2D EXSY experiments were performed using nuclear Overhauser spectroscopy (NOESY) pulse sequence; spin-saturation-transfer (SST) experiments were performed according to a literature procedure.^{70,71} Full spectra and complete characterization data for all complexes are available in the [Supporting Information](#). The signal abbreviation is as follows: s, singlet; d, doublet; t, triplet; q, quartet; quin, quintet; sept, septet; m, multiplet; br, broad; Ar-H, aromatic proton; quat, quaternary. Elemental analyses were performed using an Exeter Analytical CE440 instrument. UV-vis spectra were recorded on an Agilent Cary 60 spectrophotometer and Fourier transform infrared (FT-IR) spectra were recorded on a Cary 630 with an attenuated-total-reflectance (ATR) module. The PL measurements at varying concentrations were performed using a Hamamatsu Quantaurus-QY plus apparatus; the measurements at 298 K were performed in degassed dichloromethane solutions and at liquid nitrogen temperature in 2-methyltetrahydrofuran (MeTHF). The PL lifetime was measured using the second harmonics of a Spectra-Physics Mai Tai pulsed laser and a Hamamatsu Photonics Streak Scope camera. The decay data were fitted with a single-exponential decay function unless specified otherwise. The quantum yield was measured using a Hamamatsu Photonics Quantaurus-QY system, which established variations in the absolute QY to be within 5% for solid and solution samples (CH₂Cl₂, *c* = 1–5 μM) at 298 and 77 K. Cyclic voltammetry (CV) experiments were performed using ALS/CHI electrochemical analyzers 660E and 760E Electrochemical-grade ¹⁸Bu₄NPF₆ and ¹⁸Bu₄NBF₄ (Fluka) were used the supporting electrolytes. Electrochemical measurements were performed in an argon-filled glovebox. A platinum disk electrode (*d* = 1.6 mm) was used as the working electrode and a platinum wire as the auxiliary electrode. The nonaqueous silver-wire reference electrode assembly was filled with a 0.01 M AgNO₃/0.1 M ¹⁸Bu₄NClO₄/MeCN solution and calibrated against Cp₂Fe (Fc).

X-ray Structure Determination. The X-ray diffraction (XRD) data for the single crystals 1–10 were collected on a Rigaku XtaLab PRO instrument (*ω*-scan mode) with a PILATUS3 R 200 K hybrid pixel array detector and a MicroMax-003 microfocus X-ray tube using Mo K α (0.71073 Å) radiation at low temperature. Images were indexed and integrated using the *CrysAlisPro* data reduction package. Data were corrected for systematic errors and absorption using the *ABSPACK*

module: numerical absorption correction based on Gaussian integration over a multifaceted crystal model and empirical absorption correction based on spherical harmonics according to the point group symmetry using equivalent reflections. The *GRAL* module and *ASSIGN SPACEGROUP* routine of the *WinGX* suite⁷² were used for analysis of systematic absences and space group determination. The structures were solved by direct methods using *SHELXT*⁷³ and refined by full-matrix least squares on *F*² using *SHELXL*.⁷⁴ The non-H atoms were refined anisotropically. The H atoms were inserted at the calculated positions and refined as riding atoms. The positions of the H atoms of the methyl groups were found using rotating group refinement with idealized tetrahedral angles. Complex 6 crystallizes with two molecules A and B in the asymmetric cell (*Z'* = 2); complex 9 crystallizes with the molecule bisected by a mirror plane (*Z'* = 0.5). N4B-pivot ^{nc}Pent (symmetrically independent molecule B) and N3-pivot ⁱBu substituents of 6 and 8, respectively, are disordered into two positions. In the case of 7, the ^{sec}Bu fragment at atom N3 and the N4-^{sec}Bu moiety are involved in substitutional disordering with different configurations of chiral C atoms; the racemic composition of the whole unit cell is provided by crystallographic inversion symmetry. Interestingly, as a result of the mentioned disorder, the noncoordinated N4 atom shows either a distorted pyramidal (N41) or an almost planar (N42) configuration. The disorder was resolved using free variables and reasonable restraints on geometry and anisotropic displacement parameters. Achiral complexes 1 and 3 crystallize in the Sohncke space group *P*2₁2₁2₁, and the absolute structures of the crystals were determined by means of the Flack parameter.⁷⁵ All of the compounds studied have no unusual bond lengths and angles. Section VI of the [Supporting Information](#) contains full experimental details regarding data collection and structure determination.

Synthesis of *N,N'*-Diisobutyl-2,11-diaza[3,3](2,6)-pyridinophane (^{iBu}N4). *Synthesis of 2,6-Bis[(isobutylamino)methyl]pyridine.* To a solution of 2,6-bis(bromomethyl)pyridine (2.1 g, 7.8 mmol, 1 equiv) in MeCN (10 mL) was added dropwise the solution of isobutylamine (5.74 g, 78.5 mmol, 10 equiv) in MeCN (10 mL) over 25 min at room temperature. The mixture was stirred at room temperature for 17 h. MeCN was then removed on a rotary evaporator, and residual waxy oil was dissolved in dichloromethane and washed with concentrated aqueous potassium carbonate. The organic phase was collected, dried with sodium sulfate, and concentrated to dryness. The resulting oil was distilled under vacuum at 65 °C (120 mTorr) to give the diamine product that was used in the next step without additional purification. Yield: 1.23 g (63%). ¹H NMR (600 MHz, 25 °C, CDCl₃): δ 7.58 (t, ³J_{HH} = 7.6 Hz, *p*-H_{py}, 1H), 7.16 (d, ³J_{HH} = 7.7 Hz, *m*-H_{py}, 2H), 3.88 (s, -PyCH₂NH-, 4H), 2.46 (d, ³J_{HH} = 6.9 Hz, -NHCH₂CH-, 4H), 1.87 (s, NH-, 2H), 1.84–1.74 (m, -CH₂CH-(CH₃)₂, 2H), 0.93 (d, ³J_{HH} = 6.6 Hz, -CH(CH₃)₂-, 12H). ¹³C NMR (151 MHz, 25 °C, CDCl₃): δ 159.7 (quat, C_{py}), 136.9 (*p*-C_{py}), 120.5 (*m*-C_{py}), 57.9 (-NHCH₂CH), 55.6 (-PyCH₂NH-), 28.7 (-CH₂CH(CH₃)₂-), 20.9 (-CH(CH₃)₂-).

Synthesis of ^{iBu}N4. 2,6-Bis[(isobutylamino)methyl]pyridine (1.23 g, 4.93 mmol, 1.05 equiv) was placed in a round-bottomed flask containing 20 mL of benzene and 30 mL of a 10% Na₂CO₃ aqueous solution. The mixture was heated to 80 °C, and the solution of 2,6-bis(bromomethyl)pyridine (1.24 g, 4.69 mmol, 1 equiv) was added dropwise to the hot reaction mixture over the period of 30 min. The reaction mixture was heated at 80 °C for 16 h. After cooling to room temperature, the organic phase was collected using a separatory funnel. Evaporation of the solvent furnished a white waxy solid containing the target compound. The crude was then extracted three times with 10 mL of a 1/1 (v/v) dichloromethane/hexane mixture. The extracts were then evaporated to dryness to furnish the target macrocycle. Combined yield: 1.03 g (58%). ¹H NMR (600 MHz, 25 °C, CDCl₃): δ 7.10 (t, ³J_{HH} = 7.5 Hz, *p*-H_{py}, 2H), 6.76 (d, ³J_{HH} = 7.6 Hz, *m*-H_{py}, 4H), 3.86 (s, -PyCH₂N-, 8H), 2.56 (d, ³J_{HH} = 7.2 Hz, -NCH₂CH-, 4H), 1.98 (m, -CH₂CH(CH₃)₂, 2H), 1.08 (d, ³J_{HH} = 6.6 Hz, -CH(CH₃)₂-, 12H). ¹³C NMR (151 MHz, 25 °C, CDCl₃): δ 158.4 (quat, C_{py}), 135.5 (*p*-C_{py}), 122.8 (*m*-C_{py}), 69.0 (-NCH₂CH), 64.9 (-PyCH₂N-), 27.4 (-CH₂CH(CH₃)₂-), 21.1 (-CH(CH₃)₂-). ESI-HRMS. Calcd for

[C₂₂H₃₂N₄·H⁺]: *m/z* 353.2705. Found for C₂₂H₃₂N₄·H⁺: *m/z* 353.2702.

Synthesis of *N,N'*-Di-*sec*-butyl-2,11-diaza[3,3](2,6)-pyridinophane (^{sec}BuN4). ^{sec}BuN4 (0.200 g, 0.83 mmol, 1.0 equiv), *sec*-butyl bromide (5.7 g, 41.6 mmol, 50.0 equiv; used as racemate), anhydrous K₂CO₃ (1.38 g, 9.96 mmol, 12.0 equiv), and dry MeCN (50 mL) were charged into a 100 mL round-bottomed flask with a magnetic stirring bar. The reaction mixture was refluxed under dinitrogen for 3 days. The solution was cooled to room temperature (RT) and the solvent removed under reduced pressure. The residue was suspended in 50 mL of CH₂Cl₂ and then washed with 1 M NaOH and water. The CH₂Cl₂ layer was isolated, dried over anhydrous K₂CO₃, evaporated, and further dried under vacuum to give a pale-yellow powder. Yield: 208 mg (71%). ¹H NMR (400 MHz, 25 °C, CDCl₃): δ 7.08 (t, ³J_{HH} = 7.7 Hz, *p*-H_{Ppy}, 2H), 6.74 (d, ³J_{HH} = 7.7 Hz, *m*-H_{Ppy}, 4H), 3.96 (d, ²J_{HH} = 12.2 Hz, PyCH₂N-, 4H), 3.81 (d, ²J_{HH} = 12.2 Hz, PyCH₂N-, 4H), 2.95–2.87 (m, -NCH(CH₃)(CH₂CH₃), 2H), 1.83–1.72 (m, -CHCH₂CH₃, 2H), 1.52–1.41 (m, -CHCH₂CH₃, 2H), 1.19 (d, ³J_{HH} = 6.4 Hz, NCHCH₃, 6H), 1.10 (t, ³J_{HH} = 7.3 Hz, -CH₂CH₃, 6H). ¹³C NMR (100 MHz, 25 °C, CDCl₃): δ 159.3 (quat, C_{py}), 135.8 (*p*-C_{py}), 122.9 (*m*-C_{py}), 65.70 (-NCH(CH₃)(CH₂CH₃)), 65.67 (-NCH(CH₃)(CH₂CH₃)-), 60.9 (br, PyCH₂N-), 28.1 (-CHCH₂CH₃-), 28.0 (-CHCH₂CH₃), 15.81 (-CHCH₃), 15.76 (-CHCH₃), 12.5 (-CH₂CH₃); two sets of signals were observed in equal ratio for the N-CH C atom of the *sec*-butyl group and adjacent C atoms due to the presence of two diastereomers. ESI-HRMS. Calcd for [C₂₂H₃₂N₄·H⁺]: *m/z* 353.2700. Found for C₂₂H₃₂N₄·H⁺: *m/z* 353.2700.

Synthesis of ^{neo}PentN4. **Synthesis of 2,6-Bis[(*neo*-pentylamino)-methyl]pyridine.** 2,6-Bis(bromomethyl)pyridine (1.20 g, 4.53 mmol, 1.0 equiv) was added slowly to the *neo*-pentylamine (7.90 g, 90.6 mmol, 20.0 equiv) at RT with stirring. The mixture was stirred at room temperature for 17 h. Extra *neo*-pentylamine was then removed on a rotary evaporator, and the residual waxy oil was dissolved in dichloromethane and washed with concentrated aqueous potassium carbonate. The organic phase was collected, dried with sodium sulfate, and concentrated to dryness. The resulting waxy solid was used in the next step without additional purification. Yield: 1.24 g (98%). ¹H NMR (600 MHz, 25 °C, CDCl₃): δ 7.61 (t, ³J_{HH} = 7.6 Hz, *p*-H_{Ppy}, 1H), 7.21 (d, ³J_{HH} = 7.7 Hz, *m*-H_{Ppy}, 2H), 3.96 (s, PyCH₂NH-, 4H), 2.84 (br s, 2H), 2.43 (s, -NHCH₂C-, 4H), 0.96 (s, -CH₂C(CH₃)₃-, 18H). ¹³C NMR (151 MHz, 25 °C, CDCl₃): δ 158.9 (quat, C_{py}), 137.4 (*p*-C_{py}), 120.9 (*m*-C_{py}), 62.1 (PyCH₂NH-), 55.7 (-NHCH₂C-), 31.9 (-CH₂C(CH₃)₃), 28.2 (-CH₂C(CH₃)₃).

Synthesis of ^{neo}PentN4. 2,6-Bis[(*neo*-pentylamino)methyl]pyridine (1.24 g, 4.47 mmol, 1.0 equiv) was placed in a round-bottomed flask containing benzene (20 mL) and a 10% Na₂CO₃ (30 mL) aqueous solution. The mixture was heated to 80 °C, and the solution of 2,6-bis(bromomethyl)pyridine (1.13 g, 4.25 mmol, 0.95 equiv) was added dropwise to the hot reaction mixture over a period of 30 min. The reaction mixture was heated at 80 °C for 16 h. After cooling to room temperature, the organic phase was collected using a separatory funnel. Evaporation of the solvent furnished a white, waxy solid containing the target compound. The crude was then treated with MeCN (15 mL) and filtered to remove an insoluble white solid. The MeCN filtrate was extracted with hexane. The hexane layer was concentrated to give the target product as a white powder. Combined yield: 0.129 g (7%). ¹H NMR (400 MHz, 25 °C, CDCl₃): δ 7.11 (t, ³J_{HH} = 7.6 Hz, *p*-H_{Ppy}, 2H), 6.90 (d, ³J_{HH} = 7.7 Hz, *m*-H_{Ppy}, 4H), 3.97 (s, -PyCH₂N-, 8H), 2.58 (s, -NCH₂C-, 4H), 1.09 (s, -C(CH₃)₃-, 18H). ¹³C NMR (100 MHz, 25 °C, CDCl₃): δ 158.4 (quat, C_{py}), 135.5 (*p*-C_{py}), 122.8 (*m*-C_{py}), 72.5 (-NCH₂C-), 67.7 (PyCH₂N-), 34.2 (-C(CH₃)₃), 28.1 (-C(CH₃)₃-). ESI-HRMS. Calcd for [C₂₄H₃₇N₄·H⁺]: *m/z* 381.3013. Found for C₂₄H₃₇N₄·H⁺: *m/z* 381.3010.

General Procedure for the Synthesis of [(^RN4)Cu^I(MeCN)]X (X = PF₆, BF₄). To a stirred solution of the ligand (1.0 equiv) in MeCN was added [Cu(MeCN)₄]PF₆ or [Cu(MeCN)₄]BF₄ (1.0 equiv), which immediately produced a red-orange solution. The reaction was stirred for 30 min, filtered through a Celite plug, and then recrystallized by the slow diffusion of diethyl ether vapor over 1–2 days at room

temperature. Crystalline solids were collected, washed with ether and hexane, and dried under vacuum. Crystals suitable for X-ray analysis were obtained by diethyl ether vapor diffusion into a MeCN solution of the complex. The details are given below for individual complexes, and the full characterization is given in the [Supporting Information](#).

[(^{Pr}N4)Cu^I(MeCN)]PF₆ (1). Orange crystalline solid. Isolated yield: 111 mg (63%). At -30 °C, [(^{κ⁴-^{Pr}N4})Cu^I(MeCN)]PF₆ and [(^{κ³-^{Pr}N4})Cu^I(MeCN)]PF₆ isomers were present in a CD₃CN solution in a 93.5:6.5 ratio by NMR integration. ^{κ⁴}-1, major isomer. ¹H NMR (600 MHz, -30 °C, CD₃CN): δ 7.32 (t, ³J_{HH} = 7.7 Hz, *p*-H_{Ppy}, 2H), 6.77 (d, ³J_{HH} = 7.6 Hz, *m*-H_{Ppy}, 4H), 4.14 (d, ²J_{HH} = 15.3 Hz, -PyCH₂N-, 4H), 3.60–3.53 (m, -NCH(CH₃)₂-, 2H), 3.54 (d, ²J_{HH} = 15.3 Hz, -PyCH₂N-, 4H), 1.96 (s, CH₃CN, 3H), 1.31 (d, ³J_{HH} = 6.6 Hz, -CH(CH₃)₂-, 12H). ¹³C NMR (151 MHz, -30 °C, CD₃CN): δ 157.2 (quat, C_{py}), 137.3 (*p*-C_{py}), 122.8 (*m*-C_{py}), 58.0 (-CH(CH₃)₂-), 57.7 (-PyCH₂N-), 18.9 (-CH(CH₃)₂-). ^{κ³}-1, minor isomer. ¹H NMR (600 MHz, -30 °C, CD₃CN): δ 7.40 (t, ³J_{HH} = 7.7 Hz, *p*-H_{Ppy}, 2H), 6.99 (d, ³J_{HH} = 7.7 Hz, *m*-H_{Ppy}, 2H), 6.82 (d, ³J_{HH} = 7.7 Hz, *m*-H_{Ppy}, 2H), 4.29 (d, ²J_{HH} = 15.2 Hz, -PyCH₂N-, 2H), 4.22 (d, ²J_{HH} = 12.4 Hz, -PyCH₂N-, 2H), 4.02 (d, ²J_{HH} = 12.4 Hz, -PyCH₂N-, 2H), 3.74 (d, ²J_{HH} = 15.2 Hz, -PyCH₂N-, 2H), 1.39 (d, ³J_{HH} = 6.5 Hz, -CH(CH₃)₂-, 6H), 1.22 (d, ³J_{HH} = 6.6 Hz, -CH(CH₃)₂-, 6H). The -CH(CH₃)₂- peak could not be observed because of its low intensity. ¹³C NMR (151 MHz, -30 °C, CD₃CN): δ 159.2 (quat, C_{py}), 155.3 (quat, C_{py}), 138.3 (*p*-C_{py}), 124.9 (*m*-C_{py}), 122.4 (*m*-C_{py}), 62.5 (-PyCH₂N- or -CH(CH₃)₂-), 60.2 (-CH(CH₃)₂- or -PyCH₂N-), 59.6 (-PyCH₂N- or -CH(CH₃)₂-), 19.0 (-CH(CH₃)₂-), 18.7 (-CH(CH₃)₂-). Anal. Found (calcd for C₂₂H₃₁CuF₆N₅P): C, 45.68 (46.03); H, 5.30 (5.44); N, 11.99 (12.20).

[(^{Me}N4)Cu^I(MeCN)]BF₄ (2). Orange crystalline solid. Isolated yield: 55 mg (65%). At -26 °C, [(^{κ⁴-^{Me}N4})Cu^I(MeCN)]BF₄ and [(^{κ³-^{Me}N4})Cu^I(MeCN)]BF₄ isomers were present in a CD₃CN solution in a 96.6:3.38 ratio by NMR integration. ^{κ⁴}-2, major isomer. ¹H NMR (600 MHz, -26 °C, CD₃CN): δ 7.31 (t, ³J_{HH} = 7.5 Hz, *p*-H_{Ppy}, 2H), 6.73 (d, ³J_{HH} = 7.7 Hz, *m*-H_{Ppy}, 4H), 4.04 (d, ²J_{HH} = 15.1 Hz, -PyCH₂N-, 4H), 3.54 (d, ²J_{HH} = 15.1 Hz, -PyCH₂N-, 4H), 2.91 (s, -NCH₃, 6H), 1.97 (s, CH₃CN, 3H). ¹³C NMR (151 MHz, -26 °C, CD₃CN): δ 156.7 (quat, C_{py}), 137.7 (*p*-C_{py}), 122.8 (*m*-C_{py}), 64.6 (-PyCH₂N-), 49.0 (-NCH₃). ^{κ³}-2, minor conformer. ¹H NMR (600 MHz, -30 °C, CD₃CN): δ 7.45 (t, ³J_{HH} = 7.5 Hz, *p*-H_{Ppy}, 2H), 7.00 (d, ³J_{HH} = 7.9 Hz, *m*-H_{Ppy}, 2H), 6.89 (d, ³J_{HH} = 7.3 Hz, *m*-H_{Ppy}, 2H), 4.34 (d, ²J_{HH} = 13.5 Hz, -PyCH₂N-, 2H), 4.29 (d, ²J_{HH} = 15.6 Hz, -PyCH₂N-, 2H), 4.19 (d, ²J_{HH} = 13.5 Hz, -PyCH₂N-, 2H), 3.76 (d, ²J_{HH} = 15.6 Hz, -PyCH₂N-, 2H), 3.03 (s, -NCH₃, 6H). The ¹³C peaks of [(^{κ³-^{Me}N4})Cu^I(CH₃CN)]BF₄ could not be detected because of their low intensity. Anal. Found (calcd for C₁₈H₂₃CuF₄N₅B): C, 46.60 (47.02); H, 4.93 (5.04); N, 14.76 (15.23).

[(^HN4)Cu^I(MeCN)]PF₆ (3). Orange crystalline solid. Isolated yield: 35 mg (17%). At -30 °C, [(^{κ⁴-^HN4})Cu^I(MeCN)]PF₆ and [(^{κ³-^HN4})Cu^I(MeCN)]PF₆ isomers were present in a CD₃CN solution in a 87.3:12.7 ratio by NMR integration. ^{κ⁴}-3, major isomer. ¹H NMR (600 MHz, -30 °C, CD₃CN): δ 7.33 (t, ³J_{HH} = 7.7 Hz, *p*-H_{Ppy}, 2H), 6.81 (d, ³J_{HH} = 7.7 Hz, *m*-H_{Ppy}, 4H), 4.27 (2 doublets, ²J_{HH} = 15.9 Hz, -PyCH₂N-, 4H), 3.64 (d, ²J_{HH} = 15.9 Hz, -PyCH₂N-, 4H), 3.60 (br m, -CH₂NH, 2H), 1.96 (s, CH₃CN, 3H). ¹³C NMR (151 MHz, -30 °C, CD₃CN): δ 157.4 (quat, C_{py}), 137.1 (*p*-C_{py}), 122.6 (*m*-C_{py}), 55.8 (-PyCH₂N-). ^{κ³}-3, minor conformer. ¹H NMR (600 MHz, -30 °C, CD₃CN): δ 7.47 (t, ³J_{HH} = 7.6 Hz, *p*-H_{Ppy}, 2H), 7.06 (d, ³J_{HH} = 7.8 Hz, *m*-H_{Ppy}, 2H), 6.91 (d, ³J_{HH} = 7.7 Hz, *m*-H_{Ppy}, 2H), 4.42 (d, ²J_{HH} = 14.3 Hz, -PyCH₂N-, 2H), 4.41 (d, ²J_{HH} = 16.1 Hz, -PyCH₂N-, 2H), 4.18 (d, ²J_{HH} = 14.3 Hz, -PyCH₂N-, 2H), 3.80 (d, ²J_{HH} = 16.1 Hz, -PyCH₂N-, 2H). ¹³C NMR (151 MHz, -30 °C, CD₃CN): δ 155.7 (quat, C_{py}), 138.8 (*p*-C_{py}), 124.1 (*m*-C_{py}), 122.4 (*m*-C_{py}), 57.6 (-PyCH₂N-). Second inequivalent resonance of quat C_{py} and -PyCH₂-N groups could not be detected in ¹³C NMR because of overlap with other peaks and small intensity. Anal. Found (calcd for C₁₆H₁₉CuF₆N₅P): C, 39.02 (39.23); H, 3.71 (3.91); N, 13.79 (14.30).

[(^{ts}N4)Cu^I(MeCN)]PF₆ (**4**). Yellow crystalline solid. Isolated yield: 29 mg (20%), low yield because the product was sparingly soluble in MeCN). Complex **4** remains fluxional in a CD₃CN solution even when cooled to −30 °C. The effective symmetry of the ligand is C_{2v}, which could be due to the presence of only the κ⁴ isomer or due to a fast, unresolved exchange process. ¹H NMR (600 MHz, −30 °C, CD₃CN): δ 7.89 (d, ³J_{HH} = 7.8 Hz, −(SO₂)CCHCH−Ar, 4H), 7.66–7.42 (br m, *p*-H_{Py}, and −CHCCCH₃−Ar, 6H), 7.08–6.83 (br m, *m*-H_{Py}, 4H), 5.29 (br s, −PyCH₂N−, 4H), 3.59 (br s, −PyCH₂N−, 4H), 2.50 (s, CH₃−Ar, 6H), 1.96 (s, CH₃CN, 3H). ¹³C NMR (151 MHz, −30 °C, CD₃CN): δ 153.9 (quat, C_{Py}), 146.2 (−CHCCCH₃−Ar), 140.2 (−(SO₂)CCH−Ar), 138.9 (*p*-C_{Py}), 131.1 (CHCCCH₃−Ar), 129.1 (−(SO₂)CCHCH−Ar), 124.6 (*m*-C_{Py}), 56.8 (−PyCH₂N−), 21.5 (CH₃−Ar). Anal. Found (calcd for C₃₀H₃₁CuF₆N₅O₄PS₂): C, 44.67 (45.14); H, 3.88 (3.91); N, 8.60 (8.77).

General Procedure for the Synthesis of (R⁴N4)Cu^I (5–10). To a stirred solution of R⁴N4 (1.0 equiv) in dry tetrahydrofuran (THF) was added CuI (0.95 equiv) to immediately produce a bright-yellow suspension. Within 10 min, the suspended solids dissolved, and after 2–5 h, a bright-yellow solid appeared. THF was removed by vacuum evaporation, and dichloromethane (for R⁴N4 complexes; R = Me, ⁱBu, ^{sec}Bu, ^{neo}Pent, ⁱPr) or a dichloromethane/methanol solution (for the ^{ts}N4 complex) was added to dissolve all of the reaction mixture. The solution was passed through a Celite plug and allowed to crystallize by diethyl ether vapor diffusion over 1–2 days. Crystalline solids were collected, washed with ether and hexane, and dried under vacuum. Crystals suitable for X-ray analysis were obtained by the slow diffusion of diethyl ether vapors into dichloromethane (**5–9**) or a dichloromethane/methanol solution (**10**).

(^{Pr}N4)Cu^I (**5**). Bright-yellow crystalline solid. Isolated yield: 120 mg (76%). At −30 °C, [(κ³-^{Pr}N4)Cu^I] and [(κ⁴-^{Pr}N4)Cu^I] isomers were present in a CD₂Cl₂ solution in a 91.2:8.8 ratio by NMR integration. κ³-**5**, major isomer. ¹H NMR (600 MHz, −30 °C, CD₂Cl₂): δ 7.27 (t, ³J_{HH} = 7.7 Hz, *p*-H_{Py}, 2H), 6.89 (d, ³J_{HH} = 7.8 Hz, *m*-H_{Py}, 2H), 6.68 (d, ³J_{HH} = 7.8 Hz, *m*-H_{Py}, 2H), 4.85 (d, ²J_{HH} = 12.9 Hz, −PyCH₂N−, 2H), 4.32 (d, ²J_{HH} = 14.8 Hz, −PyCH₂N−, 2H), 3.94 (d, ²J_{HH} = 12.9 Hz, −PyCH₂N−, 2H), 3.66–3.62 (m, −CH(CH₃)₂−, 1H), 3.56 (d, ²J_{HH} = 14.8 Hz, −PyCH₂N−, 2H), 3.26–3.21 (m, −CH(CH₃)₂−, 1H), 1.46 (d, ³J_{HH} = 6.7 Hz, −CH(CH₃)₂, 6H), 1.23 (d, ³J_{HH} = 6.7 Hz, −CH(CH₃)₂, 6H). ¹³C NMR (151 MHz, −30 °C, CD₂Cl₂): δ 159.8 (quat, C_{Py}), 154.6 (quat, C_{Py}), 136.7 (*p*-C_{Py}), 124.4 (*m*-C_{Py}), 121.4 (*m*-C_{Py}), 60.1 (−PyCH₂N−), 59.9 (−PyCH₂N−), 59.4 (−CH(CH₃)₂−), 59.1 (−CH(CH₃)₂−), 19.4 (−CH(CH₃)₂), 19.2 (−CH(CH₃)₂). κ⁴-**5**, minor isomer. ¹H NMR (600 MHz, −30 °C, CD₂Cl₂): δ 7.22 (t, ³J_{HH} = 7.7 Hz, *p*-H_{Py}, 2H), 4.14 (d, ²J_{HH} = 14.8 Hz, −PyCH₂N−, 4H), 3.74–3.70 (m, −CH(CH₃)₂−, 2H), 3.42 (d, ²J_{HH} = 14.8 Hz, −PyCH₂N−, 4H), 1.32 (br d, −CH(CH₃)₂, 12H). The peaks of the meta protons of pyridine cannot be detected because of their low intensity. ¹³C NMR (151 MHz, −30 °C, CD₂Cl₂): δ 156.9 (quat, C_{Py}), 135.9 (*p*-C_{Py}), 121.9 (*m*-C_{Py}), 56.1 (−CH(CH₃)₂−). The PyCH₂N− and methyl peaks might be merging with another isomer peak. Anal. Found (calcd for CH₂Cl₂·3C₂₀H₂₈CuIN₄): C, 44.82 (44.96); H, 5.17 (5.32); N, 10.12 (10.31).

(^{neo}PentN4)Cu^I (**6**). Bright-orange crystalline solid. Isolated yield: 99 mg (66%). Complex **6** exists as a single isomer (κ³-^{neo}PentN4)Cu^I in a CD₂Cl₂ solution at −30 °C. κ³-**6**. ¹H NMR (600 MHz, −30 °C, CD₂Cl₂): δ 7.27 (t, ³J_{HH} = 7.5 Hz, *p*-H_{Py}, 2H), 7.01 (d, ³J_{HH} = 7.5 Hz, *m*-H_{Py}, 2H), 6.66 (d, ³J_{HH} = 7.5 Hz, *m*-H_{Py}, 2H), 4.94 (d, ²J_{HH} = 12.8 Hz, −PyCH₂N−, 2H), 4.45 (d, ²J_{HH} = 14.9 Hz, −PyCH₂N−, 2H), 4.08 (d, ²J_{HH} = 14.9 Hz, −PyCH₂N−, 2H), 4.01 (d, ²J_{HH} = 12.8 Hz, −PyCH₂N, 2H), 3.48 (s, −NCH₂C(CH₃)₃−, 2H), 2.55 (s, −NCH₂C(CH₃)₃−, 2H), 1.12 (s, −C(CH₃)₃, 9H), 0.99 (s, −C(CH₃)₃, 9H). ¹³C NMR (151 MHz, −30 °C, CD₂Cl₂): δ 158.4 (quat, C_{Py}), 155.5 (quat, C_{Py}), 136.7 (*p*-C_{Py}), 124.6 (*m*-C_{Py}), 121.7 (*m*-C_{Py}), 75.7 (−NCH₂C−), 71.2 (−NCH₂C−), 67.7 (−PyCH₂N), 63.7 (−PyCH₂N), 36.4 (−CH₂C(CH₃)₃), 34.2 (−CH₂C(CH₃)₃), 30.3 (−C(CH₃)₃), 27.7 (−C(CH₃)₃). Anal. Found (calcd for C₂₂H₃₂N₄CuI): C, 50.49 (50.48); H, 6.22 (6.35); N, 9.56 (9.81).

(^{sec}BuN4)Cu^I (**7**). Bright-yellow crystalline solid. Isolated yield: 64 mg (42%). Complex **7** exists as a single isomer (κ³-^{sec}BuN4)Cu^I in a CD₂Cl₂ solution at −30 °C. κ³-**7**. ¹H NMR (600 MHz, −30 °C, CD₂Cl₂): δ 7.26 (t, ³J_{HH} = 7.6 Hz, *p*-H_{Py}, 2H), 6.91 (d, ³J_{HH} = 7.6 Hz, *m*-H_{Py}, 1H), 6.85 (d, ³J_{HH} = 7.9 Hz, *m*-H_{Py}, 1H), 6.7–6.6 (m, two overlapping *m*-H_{Py}, 2H), 5.02 (dd, ²J_{HH} = 2.4 and 13.0 Hz, −PyCH₂N−, 1H), 4.76 (d, ²J_{HH} = 13.0 Hz, −PyCH₂N−, 1H), 4.32–4.24 (m, two overlapping CH₂N, 2H), 3.96–3.87 (m, two overlapping CH₂N, 2H), 3.60 (vd, ²J_{HH} = 15.0 Hz, two overlapping CH₂N, 2H), 3.28–3.23 (m, −NCH(CH₃)−(CH₂CH₃), 1H), 2.91–2.85 (m, −NCH(CH₃)(CH₂CH₃)−, 1H), 2.54–2.48 (m, −CHCH₂CH₃, 1H), 1.74–1.67 (m, −CHCH₂CH₃, 1H), 1.47–1.35 (m, −CHCH₂CH₃, 2H), 1.42 (d, ³J_{HH} = 6.7 Hz, −CHCH₃, 3H), 1.20 (d, ³J_{HH} = 6.5 Hz, −CHCH₃−, 3H), 1.01 (t, ³J_{HH} = 7.4 Hz, −CH₂CH₃, 3H), 1.00 (t, ³J_{HH} = 7.3 Hz, −CH₂CH₃, 3H); four partially overlapping signals of *m*-H of Py and eight signals for PyCH₂− arms are observed because of the asymmetric environment caused by the presence of *sec*-butyl and κ³ coordination of the ligand. ¹³C NMR (151 MHz, −30 °C, CD₂Cl₂): δ 159.97, 159.92, 159.88 (quat, C_{Py}; two signals are not resolved due to overlap), 154.79, 154.70, 154.65, 154.56 (quat, C_{Py}), 136.69 (*p*-C_{Py}), 124.60, 124.53, 124.46, 124.39 (*m*-C_{Py}), 121.57, 121.49, 121.41, 121.33 (*m*-C_{Py}), 66.39, 65.52 (−NCHCH₃), 62.94, 62.82, 60.89 (br), 59.53 (br), 58.25, 58.12 (−PyCH₂N), 27.63, 27.62 (−CH₂CH₃), 15.83, 15.61 (−CHCH₃), 11.87 (−CH₂CH₃); because of the asymmetric environment caused by *sec*-butyl groups and the presence of two diastereomers, four sets of signals were observed for meta and para protons of Py and several overlapping sets of signals for aliphatic protons. Anal. Found (calcd for C₂₂H₃₂N₄CuI): C, 48.30 (48.67); H, 5.80 (5.94); N, 10.02 (10.32).

(ⁱBuN4)Cu^I (**8**). Bright-yellow crystalline solid. Isolated yield: 78 mg (51%). Complex **6** exists as a single isomer (κ³-ⁱBuN4)Cu^I in a CD₂Cl₂ solution at −30 °C. κ³-**8**. ¹H NMR (600 MHz, −30 °C, CD₂Cl₂): δ 7.30 (t, ³J_{HH} = 7.6 Hz, *p*-H_{Py}, 2H), 6.84 (d, ³J_{HH} = 7.6 Hz, *m*-H_{Py}, 2H), 6.73 (d, ³J_{HH} = 7.5 Hz, *m*-H_{Py}, 2H), 4.94 (d, ²J_{HH} = 13.5 Hz, −PyCH₂N−, 2H), 4.35 (d, ²J_{HH} = 15.1 Hz, −PyCH₂N−, 2H), 4.05 (d, ²J_{HH} = 13.5 Hz, −PyCH₂N−, 2H), 3.85 (d, ²J_{HH} = 15.1 Hz, −PyCH₂N−, 2H), 3.30 (d, ³J_{HH} = 6.3 Hz, −NCH₂CH−, 2H), 2.41 (d, ³J_{HH} = 7.3 Hz, −NCH₂CH−, 2H), 2.32–2.26 (m, −CH₂CH(CH₃)₂, 1H), 2.01–1.95 (m, −CH₂CH(CH₃)₂, 1H), 1.09 (d, ³J_{HH} = 6.8 Hz, −CH(CH₃)₂, 6H), 0.99 (d, ³J_{HH} = 6.6 Hz, −CH(CH₃)₂, 6H). ¹³C NMR (151 MHz, −30 °C, CD₂Cl₂): δ 156.9 (quat, C_{Py}), 155.0 (quat, C_{Py}), 136.4 (*p*-C_{Py}), 124.0 (*m*-C_{Py}), 121.3 (*m*-C_{Py}), 71.3 (−NCH₂CH−), 63.7 (−NCH₂CH− and −PyCH₂C), 63.3 (−PyCH₂C), 26.9 (−CH₂CH(CH₃)₂), 26.1 (−CH₂CH(CH₃)₂), 22.8 (−CH(CH₃)₂), 20.4 (−CH(CH₃)₂). Anal. Found (calcd for C₂₃H₃₄N₄CuI): C, 48.72 (48.67); H, 5.89 (5.94); N, 10.35 (10.32).

(^{Me}N4)Cu^I (**9**). Bright-yellow crystalline solid. Isolated yield: 101 mg (59%). At −30 °C, [(κ⁴-^{Me}N4)Cu^I] and [(κ³-^{Me}N4)Cu^I] isomers were present in a CD₂Cl₂ solution in a 63.5:36.5 ratio by NMR integration. κ⁴-**9**, major isomer. ¹H NMR (600 MHz, −30 °C, CD₂Cl₂): δ 7.20 (t, ³J_{HH} = 7.9 Hz, *p*-H_{Py}, 2H), 6.61 (d, ³J_{HH} = 7.4 Hz, *m*-H_{Py}, 4H), 4.03 (d, ²J_{HH} = 14.8 Hz, −PyCH₂N−, 4H), 3.40 (d, ²J_{HH} = 14.8 Hz, −PyCH₂N−, 4H), 2.90 (s, −NCH₃, 6H). ¹³C NMR (151 MHz, −30 °C, CD₂Cl₂): δ 156.2 (quat, C_{Py}), 136.0 (*p*-C_{Py}), 121.8 (*m*-C_{Py}), 64.5 (−PyCH₂N−), 50.1 (−NCH₃). κ³-**9**, minor conformer. ¹H NMR (600 MHz, −30 °C, CD₂Cl₂): δ 7.32 (t, ³J_{HH} = 7.7 Hz, *p*-H_{Py}, 2H), 6.88 (d, ³J_{HH} = 7.4 Hz, *m*-H_{Py}, 2H), 6.75 (d, ³J_{HH} = 7.4 Hz, *m*-H_{Py}, 2H), 4.92 (d, ²J_{HH} = 13.6 Hz, −PyCH₂N−, 2H), 4.79 (d, ²J_{HH} = 15.3 Hz, −PyCH₂N−, 2H), 4.02 (d, ²J_{HH} = 13.6 Hz, −PyCH₂N−, 2H), 3.62 (d, ²J_{HH} = 15.3 Hz, −PyCH₂N−, 2H), 3.02 (s, −NCH₃, 3H), 2.51 (s, −NCH₃, 3H). ¹³C NMR (151 MHz, −30 °C, CD₂Cl₂): δ 155.6 (quat, C_{Py}), 154.8 (quat, C_{Py}), 136.4 (*p*-C_{Py}), 124.1 (*m*-C_{Py}), 121.3 (*m*-C_{Py}), 66.2 (−PyCH₂N−), 64.9 (−PyCH₂N−), 50.7 (−NCH₃), 43.9 (−NCH₃). Anal. Found (calcd for C₁₆H₂₀N₄CuI): C, 41.77 (41.89); H, 4.40 (4.39); N, 11.88 (12.21).

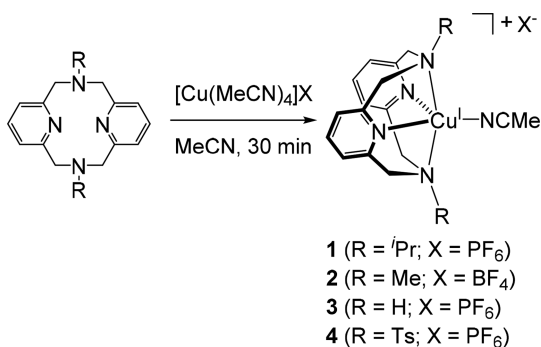
(^{ts}N4)Cu^I (**10**). Bright-yellow crystalline solid. Isolated yield: 41 mg (30%, low yield due to low solubility in dichloromethane). In CD₂Cl₂, complex **10** remains fluxional even at −80 °C. The effective symmetry of the ligand is C_{2v}, which could be due to either the presence of only

one isomer, (κ^4 -TsN4)Cu^I or (κ^2 -TsN4)Cu^I, or due to unresolved fast exchange. Single isomer. ¹H NMR (600 MHz, −80 °C, CD₂Cl₂): δ 7.71 (d, ³J_{HH} = 7.7 Hz, −(SO₂)CCHCH−_{Ar}, 4H), 7.38 (d, ³J_{HH} = 7.7 Hz, −CHCCH₃−_{Ar}, 4H), 7.32 (t, ³J_{HH} = 7.3 Hz, *p*-H_{py}, 2H), 7.06 (br s, *m*-H_{py}, 4H), 5.01 (br d, ²J_{HH} = 11.2 Hz, −PyCH₂N−, 4H), 3.60 (br d, ²J_{HH} = 11.2 Hz, −PyCH₂N−, 4H), 2.41 (s, CH₃−_{Ar}, 6H). ¹³C NMR (151 MHz, −80 °C, CD₂Cl₂): δ 154.2 (quat, C_{py}), 143.8 (CHCCH₃−_{Ar}), 137.0 (*p*-C_{py}), 134.2 (−(SO₂)CCH−_{Ar}), 129.7 (−CHCCH₃−_{Ar}), 126.5 (−(SO₂)CCHCH₃−_{Ar}), 122.8 (*m*-C_{py}), 56.0 (−PyCH₂N−), 21.2 (CH₃−_{Ar}). Anal. Found (calcd for CH₂Cl₂·C₂₈H₂₈CuIN₄O₄S₂): C, 42.17 (42.27); H, 3.65 (3.67); N, 6.53 (6.80).

RESULTS AND DISCUSSION

Synthesis and Solid-State Structures. Cationic Complexes. Cationic copper(I) complexes with a series of pyridinophane ligands were synthesized by reacting [Cu(MeCN)₄]⁺X[−] (X = PF₆, BF₄) with 1 equiv of the pyridinophane ligand (Scheme 2); they were isolated in an analytically pure

Scheme 2. Synthesis of Cationic Copper(I) Complexes



form as orange (1–3) or yellow (4) crystalline solids in 17–66% yield. All of these complexes were completely soluble in polar solvents such as CH₃CN and acetone and poorly soluble in nonpolar solvents. All [(^RN4)Cu^I(MeCN)]PF₆/BF₄ (1–4) complexes reacted slowly with chlorinated solvents, CH₂Cl₂ and CHCl₃, to form the respective (^RN4)Cu^{II} chloride complexes. All cationic complexes were highly unstable in the presence of air both in solution and in the solid state. All obtained complexes

were characterized by elemental analysis, NMR, UV–vis, and FT-IR spectroscopy, and their solid-state structures were determined by single-crystal XRD (Figure 1). Although complex 2 with a PF₆[−] counterion did not yield crystals suitable for X-ray analysis, the analogous complex 2 with BF₄[−] as a counterion was analyzed by XRD. The attempted preparation of the cationic complex with ^tBuN4 failed to give the desired product in an analytically pure form under the same conditions even after multiple recrystallizations.

X-ray analysis reveals that the pyridinophane ligand ^RN4 adopts a *syn*-boat–boat conformation^{62,63} in cationic copper(I) complexes, featuring stronger coordination of the two pyridine rings and one MeCN ligand and weaker interactions with the two axial amines. The coordination geometry of the Cu centers can be formally described as distorted square-pyramidal,⁶¹ with τ_5 parameter values closer to 0 expected from the ideal square-pyramidal geometry; however, the Cu–N_{amine} distances are significantly elongated compared to the Cu–N_{py} distances. A comparison of the bond distances in complexes [(^RN4)Cu^I(MeCN)]⁺ 1–4 given in Table 1 shows that the Cu–N_{py} and Cu–N_{MeCN} bond distances are in a range of 1.88–2.10 Å typical for Cu–N bond lengths,^{60,61,76–79} while the Cu–N_{amine} distances are significantly longer (Cu–N_{amine} 2.35–2.49 Å). These structures resemble those previously reported for other ^RN4-type pyridinophanecopper(I) complexes.^{60,61} The comparison of two analogous cationic complexes with different counteranions, [(^tBuN4)Cu^I(MeCN)](PF₆) and [(^tBuN4)Cu^I(MeCN)](BF₄), shows that bond distances and coordination geometries are quite similar for both complexes.

The comparison of Cu–N_{amine} bond lengths (Cu1–N3 and Cu1–N4, Table 1) in complexes [(^RN4)Cu^I(MeCN)]X (1–4) as well as a comparison with the published structures of [(^tBuN4)Cu^I(MeCN)]X with bulky ^tBu groups at the amines reveals that greater steric hindrance at the axial amine substituents leads to noticeable elongation of the Cu–N_{amine} bond lengths in the following order: R = ^tBu > ⁱPr > Me > H. At the same time, complex 4 with a Ts-substituted amine features the longest Cu–axial amine distances, likely due to weak interactions with poorly donating N–Ts groups.

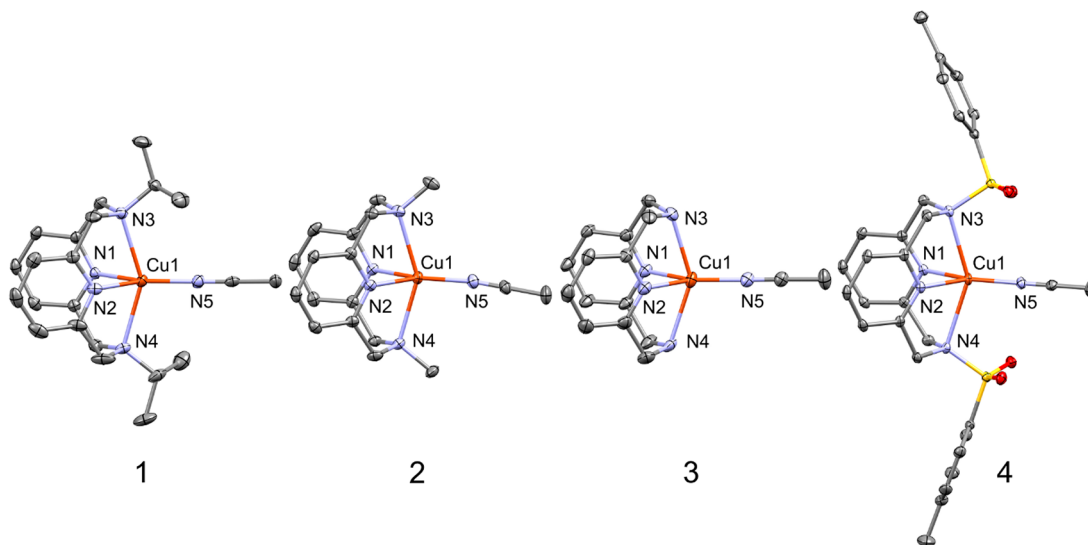


Figure 1. ORTEP projections of MeCN complexes 1–4 showing anisotropic displacement ellipsoids at the 50% probability level. H atoms and counterions are omitted for clarity.

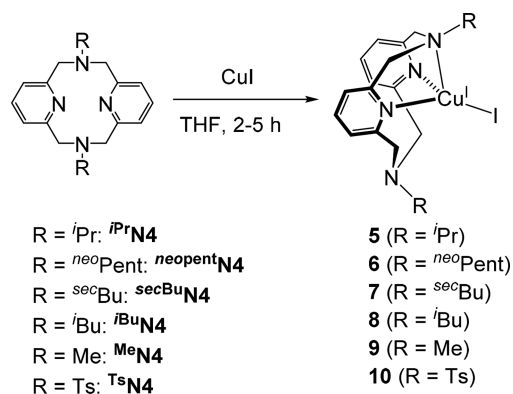
Table 1. Selected Cu–N Bond Distances and τ_5 Geometrical Indices^a in Complexes [(^RN4)Cu^I(MeCN)]X (1–4) and [(ⁱBuN4)Cu^I(MeCN)]X (X = PF₆, BF₄)

complex	Cu1–N1, Å	Cu1–N2, Å	Cu1–N3, Å	Cu1–N4, Å	Cu1–N5, Å	τ_5^a
[(ⁱ BuN4)Cu ^I (MeCN)](PF ₆) ^b	2.089(2)	2.099(2)	2.444(2)	2.470(2)	1.901(2)	0.04
[(ⁱ BuN4)Cu ^I (MeCN)](BF ₄) ^b	2.0920(18)	2.0819(16)	2.4249(16)	2.4570(17)	1.8957(19)	0.08
[(^{Pr} N4)Cu ^I (MeCN)](PF ₆) (1)	2.098(3)	2.082(3)	2.418(3)	2.400(3)	1.890(3)	0.14
[(^{Me} N4)Cu ^I (MeCN)](BF ₄) (2)	2.0782(10)	2.0784(10)	2.3722(10)	2.3577(10)	1.8804(10)	0.03
[(^H N4)Cu ^I (MeCN)](PF ₆) (3)	2.0892(15)	2.0937(16)	2.3510(17)	2.3653(17)	1.8824(16)	0.13
[(^{Ts} N4)Cu ^I (MeCN)](PF ₆) (4)	2.0641(11)	2.0749(11)	2.4219(11)	2.4902(11)	1.8828(12)	0.15

^aThe geometrical indices τ_5 for pentacoordinate structures are calculated according to refs 80–82. ^bFrom ref 60, the atom numbering corresponds to that from Figure 1.

The ATR FT-IR spectra of polycrystalline samples of complexes 1, 3, and 4 are consistent with the presence of a noncoordinated PF₆[−] counterion characterized by the 820–831 cm^{−1} band, while complex 2 shows bands between 1047 and 1003 cm^{−1} that are typical for the BF₄[−] counterion. The N–H stretching bands of the ^HN4 ligand appear at 3400 cm^{−1} for complex 3. For complex 4, the characteristic S=O and N–S stretching bands appear at 1088 and 992 cm^{−1}, respectively.

Neutral Copper(I) Iodide Complexes. The neutral copper(I) iodide complexes were synthesized by mixing pyridinophane ligands with anhydrous copper iodide in dry THF to provide yellow (5 and 7–10) and orange (6) complexes (^RN4)Cu^I (Scheme 3), which were isolated in an analytically pure form in

Scheme 3. Synthesis of Neutral Copper(I) Iodide Complexes

15–76% yields and characterized by elemental analysis, NMR, and FT-IR spectroscopy. All of these complexes were completely soluble in CH₂Cl₂ and acetone and poorly soluble in nonpolar solvents such as hexane, toluene, benzene, and diethyl ether. These complexes show some limited stability in the crystalline state under air but decompose in solution in the presence of oxygen. The ligand ^HN4 failed to give the desired product in a pure form under the same reaction conditions: a mixture of several complexes was obtained. Although the presence of the desired product (^HN4)Cu^I was confirmed by XRD, it could not be separated from undesired byproducts and could not be fully characterized.⁸³

The X-ray crystal structures of complexes (^RN4)Cu^I (5–10) display distorted tetrahedral coordination geometry around the Cu^I center, with the pyridinophane ligand binding in a κ^3 fashion (Figure 2). The τ_4 and τ_4' parameters for tetra-coordinate Cu centers in these complexes are in the range 0.53–0.68, indicative of a noticeable deviation from the ideal tetrahedral geometry where τ_4 and τ_4' values equal to 1 are expected. In all complexes, the pyridinophane ligand adopts a *syn*-boat–chair conforma-

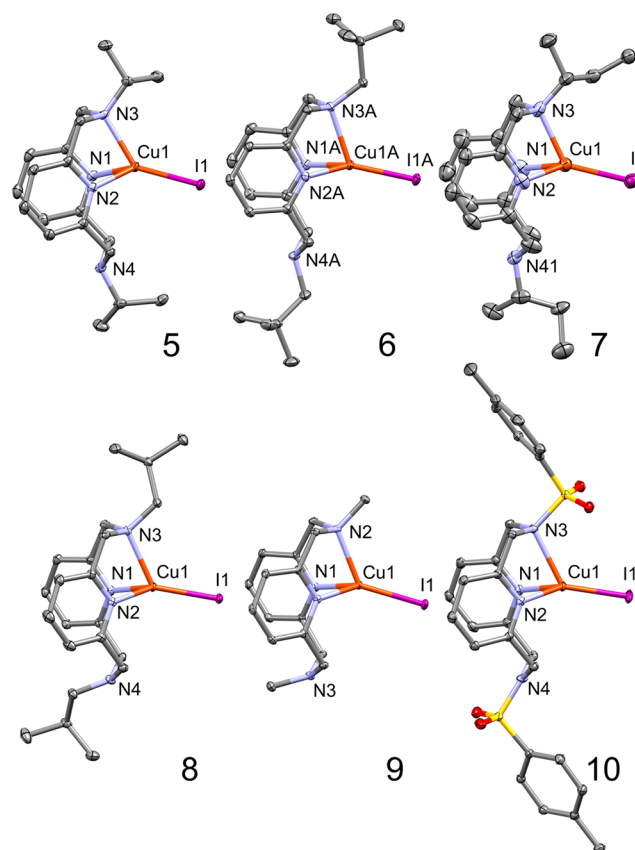


Figure 2. ORTEP projections of iodide complexes (^RN4)Cu^I (5–10) showing anisotropic displacement ellipsoids at the 50% probability level if not indicated otherwise. For complex 6, only one independent molecule A is shown. For complex 7, displacement ellipsoids are shown at the 30% probability level for clarity. H atoms, minor components of disorder, and a solvent molecule in the case of 10 are omitted for clarity.

tion. These structures also resemble the previously reported tetra-coordinate (ⁱBuN4)Cu^I (A; Scheme 1a).⁶⁰ The selected bond lengths for complexes 5–8 and a previously reported tetra-coordinate complex A with a ⁱBu-substituted pyridinophane ligand are summarized in Table 2. The Cu–axial amine distances in the solid state vary from 2.065 to 2.155 Å; however, no clear correlation with the steric properties of the alkylamine is observed, which could reflect the effect of crystal packing and intermolecular interactions, especially in the complexes where a remote steric hindrance is present, (ⁱBuN4)Cu^I and 6. It should be noted that the ^{sec}Bu and ⁱBu fragments at atom N3 for complexes 7 and 8 are disordered into two positions. Similar to complexes with alkyl-substituted ligands, 10 features a much

Table 2. Selected Cu–N and Cu–I Bond Distances and Geometrical Indices (τ_4 and τ_4') in Complexes 5–10 and A

complex	CuI–N1, Å	CuI–N2, Å	CuI–N3, Å	CuI–I1, Å	τ_4 and τ_4' values ^a	
					τ_4	τ_4'
(^t BuN4)CuI (A) ^b	2.1292(16)	2.1518(15)	2.2158(16)	2.4907(3)	0.67	0.66
(ⁱ PrN4)CuI (5)	2.1554(16)	2.1118(15)	2.2068(15)	2.4881(2)	0.62	0.60
(^{neo} PentN4)CuI (6A) ^c	2.1163(12)	2.1025(12)	2.2404(12)	2.46511(19)	0.63	0.62
(^{neo} PentN4)CuI (6B) ^c	2.1136(12)	2.0688(12)	2.2560(12)	2.46202(19)	0.62	0.53
(^{sec} BuN4)CuI (7)	2.120(5)	2.117(5)	2.234(5)	2.4737(8)	0.66	0.62
(^t BuN4)CuI (8)	2.0658(10)	2.0555(10)	2.2487(11)	2.46123(18)	0.68	0.64
(^{Me} N4)CuI (9)	2.0876(13)	2.1978(17) ^d		2.4755(3)	0.68	0.68
(^{Ts} N4)CuI (10)	2.0967(16)	2.0849(16)	2.3467(17)	2.4600(3)	0.65	0.61

^aThe geometrical indices τ_4 and τ_4' for tetracoordinate structures are calculated according to refs 80–82. ^bFrom ref 60, the atom numbering corresponds to Figure 2. ^cThere are two molecules present in the asymmetric part of the unit cell. ^dThe distance is related to the Cu–N_{amine} bond (see the numbering in Figure 2). Complex 9 crystallizes with the molecule bisected by a mirror plane; hence, the asymmetric cell contains half a molecule.

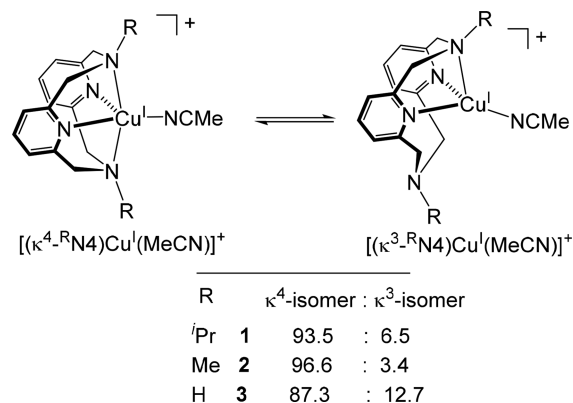
longer Cu–axial amine bond owing to weak coordination of the tosylamide N atom.

Macrocyclic Ligand Conformational Flexibility in Solution and NMR Studies. Cationic Complexes. The dynamic behavior of the complexes was investigated by a solution VT NMR study. Complexes [(^RN4)Cu^I(MeCN)]X (X = PF₆, BF₄), where R = ⁱPr (1), Me (2), and H (3), all featured slightly broadened ¹H resonances at RT indicative of the effective C_{2v} symmetry in solution. However, when the temperature was lowered to –30 °C, two isomers could be distinguished in solution under slow exchange conditions with clearly resolved, sharp proton resonances, except for complex 4, which remains fluxional (vide infra). The major isomer was assigned as a C_{2v}-symmetric [(κ^4 -^RN4)Cu^I(MeCN)]⁺, in which the ^RN4 ligand adopts a *syn*-boat–boat conformation binding to the Cu center with both pyridine and both axial amine N atoms. This is evident from the presence of only one pair of doublets of the CH₂ groups showing geminal coupling (*J* ≈ 15 Hz) and only one aromatic doublet of the pyridine meta proton (H_{meta}) integrating as 2:1 relative to the triplet of the para proton of the pyridine, H_{para}. The minor isomer was assigned as the complex [(κ^3 -^RN4)Cu^I(MeCN)]⁺, where the ligand coordinates only with three N atoms of pyridinophane, while one of the axial amines remains free. Accordingly, the CH₂ groups feature two pairs of geminally coupled doublets and two inequivalent pyridine H_{meta} resonances are observed, consistent with an effective C_s symmetry of the ligand in solution. The ratio of [(κ^4 -^RN4)Cu^I(MeCN)]⁺ to [(κ^3 -^RN4)Cu^I(MeCN)]⁺ at –30 °C is dependent on the axial amine substituent; however, in all cases, the [(κ^4 -^RN4)Cu^I(MeCN)]⁺ isomer remains predominant (Scheme 4).

Complex 4 remains highly fluxional in solution even at –30 °C featuring broad, unresolved signals of methylene protons and pyridyl aromatic protons. This is consistent with fast configurational exchange due to the weak interactions of the Cu center with poorly donating NTs axial donor groups that were observed in the solid state.

Neutral Copper(I) Iodide Complexes. The solution behavior and exchange processes were studied in more detail for the series of copper iodide complexes (^RN4)CuI (5–10; R = ^tBu, ⁱPr, ^{neo}Pent, ^{sec}Bu, ^tBu, Me). In contrast to the cationic complexes, the copper(I) iodide series displays PL not only in the solid state but also in solution. The PL properties are likely strongly affected by the complexes' fluxional behavior (vide infra).

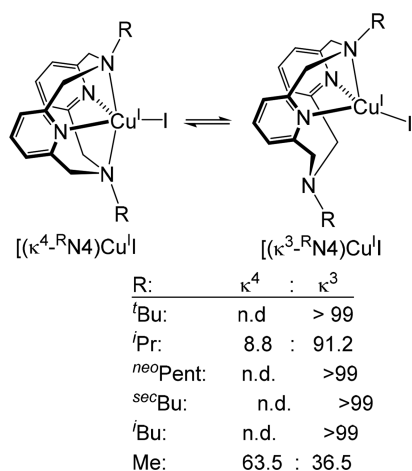
All above-mentioned complexes 5–10 are fluxional at RT featuring significantly broadened ligand resonances, which can

Scheme 4. Isomers of [(^RN4)Cu^I(MeCN)]⁺ (R = ⁱPr, Me, H) Present in a MeCN Solution at –30 °C

be resolved upon cooling, with the coalescence temperature-dependent on the substituent. The predominant isomer for complexes (^RN4)CuI (R = ^tBu, ⁱPr, ^{neo}Pent, ^{sec}Bu, ^tBu) in a CD₂Cl₂ solution was a pseudotetrahedral complex (κ^3 -^RN4)-CuI, in which the pyridinophane ligand binds only by three N atoms, while one of the amine arms remains free. In the case of ⁱPr-substituted complex 5, the minor isomer, (κ^4 -ⁱPrN4)CuI, was also present in solution, with a (κ^4 -ⁱPrN4)CuI/(κ^3 -ⁱPrN4)CuI ratio of 8.8:91.2. By contrast, complex 9 with the less sterically demanding Me-substituted ligand ^{Me}N4 shows the opposite conformational preference, with the (κ^4 -^{Me}N4)CuI complex being the predominant isomer with a (κ^4 -^{Me}N4)CuI/(κ^3 -^{Me}N4)CuI ratio of 63.5:36.5 (Scheme 5).

To further study the nature of processes involved in conformational exchange in complexes (^RN4)CuI, 2D EXSY/NOESY NMR measurements were performed at low temperature under slow exchange conditions. Although the ¹H NMR spectrum of 8, measured at –20 °C, features only one conformer, (κ^3 -^tBuN4)CuI, the EXSY spectrum clearly reveals the exchange cross peaks between two inequivalent resonances of pyridine meta protons H_m and H_{m'} that appear in the same phase as the diagonal peaks (Figure 3). In addition, exchange cross peaks are also present between two pairs of methylene doublets, H_a/H_b and H_{a'}/H_{b'}, that belong to CH₂ groups of the coordinated and noncoordinated axial amines (Figure 3). Accordingly, exchange cross peaks are also seen between two sets of corresponding multiplets of the isobutyl groups. This is indicative of the degenerative mutual-site exchange process

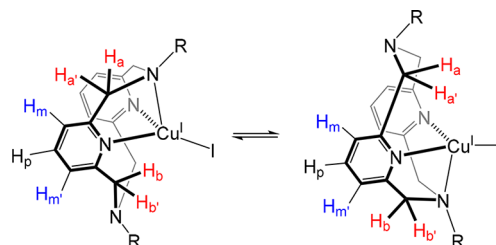
Scheme 5. Isomers of $(\kappa^3\text{-}^{\text{R}}\text{N4})\text{Cu}^{\text{I}}\text{I}$ Present in a CD_2Cl_2 Solution ($\text{R} = \text{tBu}, \text{iPr}, \text{neoPent}, \text{secBu}, \text{iBu}, \text{Me}$) at -30°C



involving coordinated and free amine arms in complex $(\kappa^3\text{-tBuN4})\text{Cu}^{\text{I}}\text{I}$, as shown in Scheme 6. Upon warming, coalescence is observed between the resonances of H_m and H_m' , which merge into a single broad signal at ca. 23°C (Figure 4).

Similar exchange peaks were also observed by EXSY at -20°C in complexes A, 6, and 7 and for a major isomer of 5 containing a κ^3 -bound iPrN4 ligand. However, the coalescence temperature for H_m and H_m' in these systems is higher compared

Scheme 6. Exchange Process in a Solution of 5–10 Involving Coordinated and Noncoordinated Amines ($\text{R} = \text{tBu}, \text{iPr}, \text{neoPent}, \text{secBu}, \text{iBu}, \text{Me}$)



to that of the less bulky complex 6. Accordingly, in iPr -substituted complex 5, the coalescence temperature is ca. 35°C , 6 showed a coalescence temperature at ca. 30°C , and in tBu -substituted complex A and secBu -substituted complex 7, coalescence was not observed even at 35°C . Because the chemical shift difference between H_m and H_m' remains similar (126 Hz) both for complexes A and 5,⁸⁴ this indicates that complex A with a more bulky tBu substituent is less fluxional in solution compared to 5.

This was further confirmed by VT SST NMR experiments in the case of complexes A, 8, and 6 featuring a simple mutual-site exchange process.⁸⁵ The SST experiment was performed by irradiating one of the doublets of the meta protons, which leads to a decrease in the intensity of the signal of the second meta proton, with the degree of suppression determined by the rate constant of exchange (Tables 3–5). The activation parameters

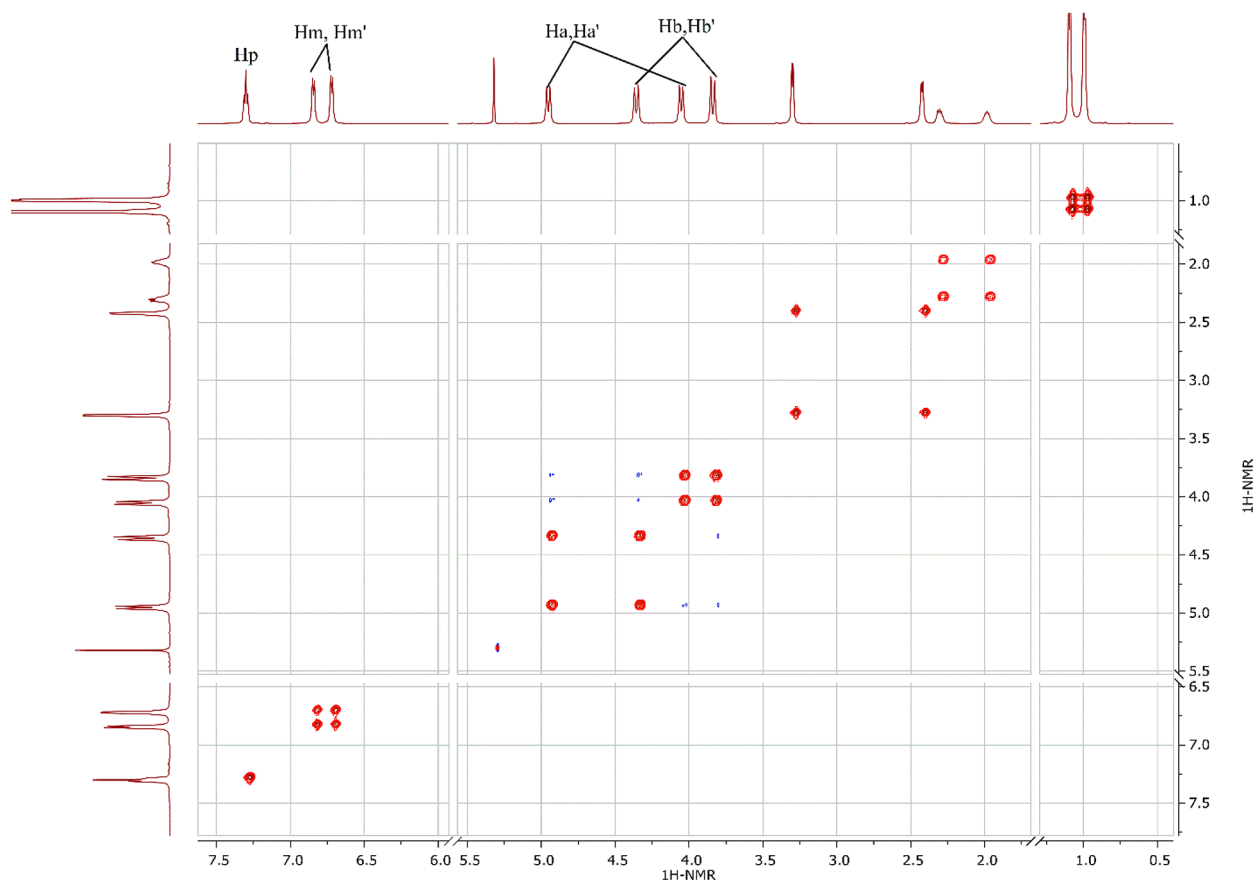


Figure 3. EXSY spectrum of complex 8 at -20°C (mixing time 0.2 s). Exchange cross peaks are shown in red, in the same phase as the diagonal peaks (NOE cross peaks are shown in blue, in the opposite phase to the diagonal peaks).

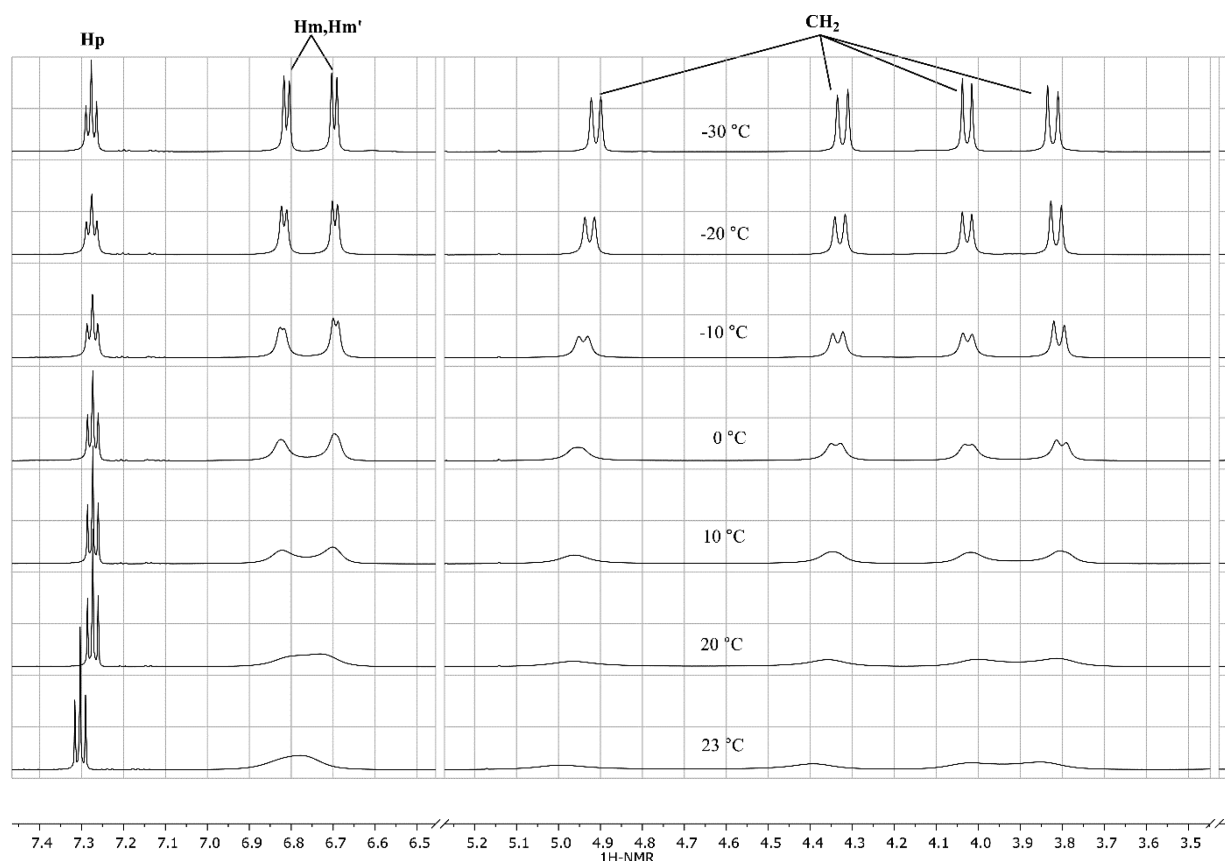


Figure 4. ^1H VT NMR spectra of complex **8** in CD_2Cl_2 .

Table 3. Rate Constant at Various Temperatures for Complex **A** in CD_2Cl_2

temperature (K)	rate constant (k , s^{-1})	temperature (K)	rate constant (k , s^{-1})
263	5.37	243	1.14
258	3.66	238	0.839
253	2.57	233	0.591
248	1.61		

Table 4. Rate Constants at Various Temperatures for Complex **8** in CD_2Cl_2

temperature (K)	rate constant (k , s^{-1})	temperature (K)	rate constant (k , s^{-1})
253	12.4	238	4.62
248	8.52	235.5	3.98
243	6.86	233	3.56
240.5	5.47	230.5	3.07

Table 5. Rate Constants at Various Temperatures for Complex **6** in CD_2Cl_2

temperature (K)	rate constant (k , s^{-1})	temperature (K)	rate constant (k , s^{-1})
255	7.15	247	3.26
253	5.88	243	2.07
251	4.73	241	1.74
249	4.06		

are given in Table 6. Complex **A** was the least fluxional among the series, while complexes featuring remote steric hindrance in

Table 6. Activation Parameters for Complexes **A**, **8**, and **6** Determined from VT SST Experiments^a

	A	8	6
ΔH^\ddagger (kcal mol^{-1})	8.5 ± 0.8	6.7 ± 0.6	11.9 ± 0.5
ΔS^\ddagger (cal $\text{mol}^{-1} \text{K}^{-1}$)	-23 ± 3	-27 ± 2	-7.4 ± 2.1
ΔG^\ddagger (kcal mol^{-1}) ^b	15.3 ± 0.8	14.7 ± 0.6	14.2 ± 0.5
E_A (kcal mol^{-1}) ^c	9.0 ± 0.8	7.2 ± 0.6	12.4 ± 0.5
$\ln A$ ^d	19 ± 2	17 ± 1	26 ± 1

^aAll experiments were repeated three times at each temperature; see details in the Supporting Information. ^bBecause measurements could not be done at RT directly, ΔG^\ddagger was extrapolated to 298 K by using the ΔH^\ddagger and ΔS^\ddagger values obtained above. ^cArrhenius activation energy. ^dNatural logarithm of the preexponential factor.

the isobutyl and *neo*-pentyl groups, **8** and **6**, showed generally faster isomer exchange rates.

As discussed above, complex **9** features two isomers in solution, $(\kappa^4\text{-MeN4})\text{CuI}$ and $(\kappa^3\text{-MeN4})\text{CuI}$, in comparable amounts, which allows for the observation of two types of exchange by EXSY NMR at -20°C . First, similar to complexes **5**, **8**, and **A**, the degenerative exchange between coordinated and noncoordinated amines is evident in the $(\kappa^3\text{-MeN4})\text{CuI}$ isomer, with the coalescence between H_m and $\text{H}_{m'}$ observed at ca. 15°C , showing that the Me-substituted complex undergoes faster conformational exchange compared to the bulkier ^{*i*}Pr-, ^{*neo*}Pent-, ^{*sec*}Bu-, and ^{*t*}Bu-substituted analogues **A** and **5–8**. The EXSY experiment also exhibits interconversion that occurs between the complexes with two different conformers of the ligand, $(\kappa^4\text{-MeN4})\text{CuI}$ and $(\kappa^3\text{-MeN4})\text{CuI}$ (Figure 5). For example, exchange cross peaks are observed between two para protons of pyridines, H_p and $\text{H}_{p'}$, that belong to isomers

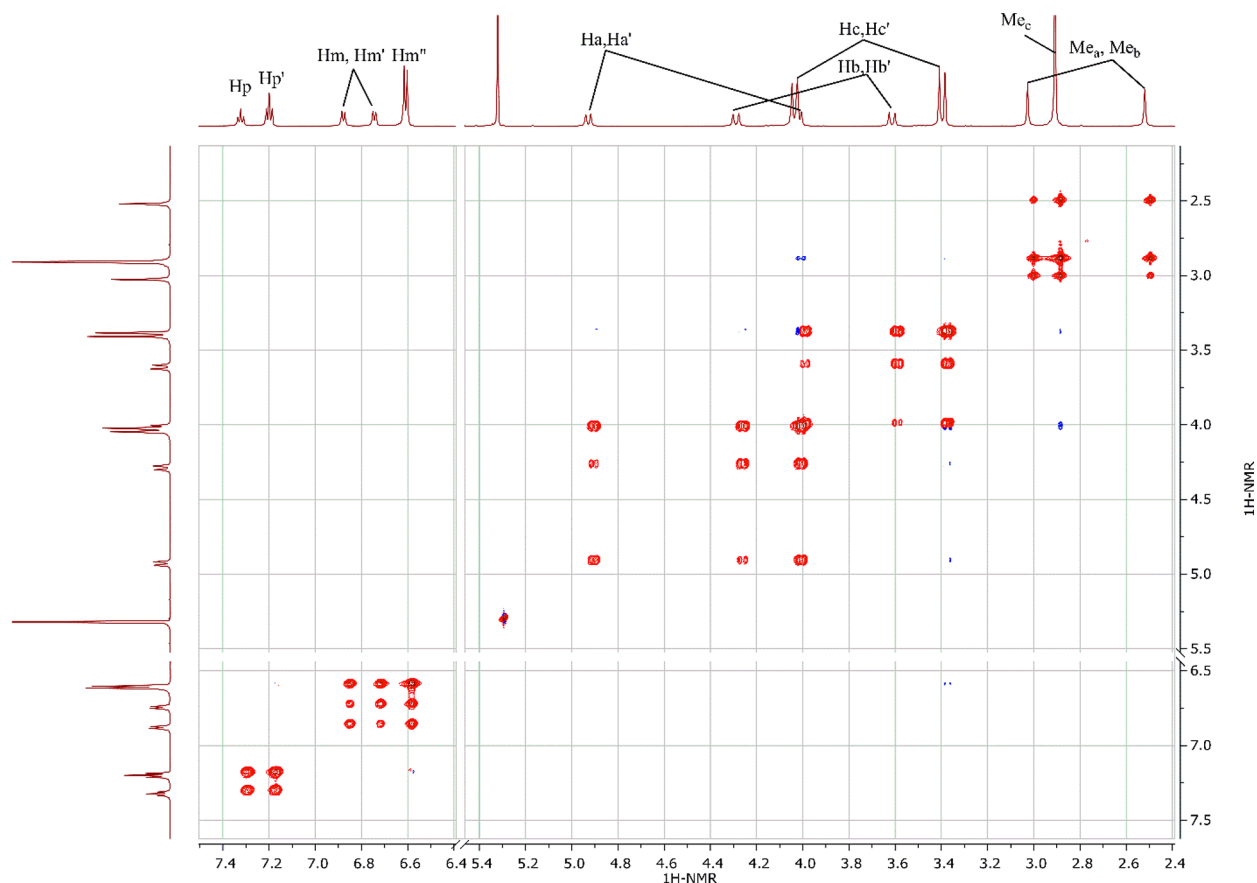
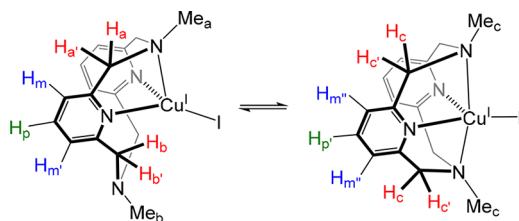


Figure 5. EXSY spectrum of complex **9** at $-20\text{ }^{\circ}\text{C}$ (mixing time of 0.2 s). Exchange cross peaks are shown in red in the same phase as the diagonal peaks (NOE cross peaks are shown in blue in the opposite phase to the diagonal peaks).

($\kappa^3\text{-MeN4}$)Cu^I and ($\kappa^4\text{-MeN4}$)Cu^I, respectively. Accordingly, both meta protons of pyridines in ($\kappa^3\text{-MeN4}$)Cu^I, H_m and $H_{m'}$, exchange, with the signal of $H_{m''}$, corresponding to pyridine meta protons of the C_{2v} -symmetrical isomer ($\kappa^4\text{-MeN4}$)Cu^I (Scheme 7). Similarly, exchange cross peaks are clearly seen between N–

Scheme 7. Isomer Interconversion Involving ($\kappa^3\text{-MeN4}$)Cu^I and ($\kappa^4\text{-MeN4}$)Cu^I



Me groups that belong to the κ^3 and κ^4 isomers, Me_a , Me_b , and Me_c . Upon warming, the resonances of N–Me of both isomers coalesce at ca. $21\text{ }^{\circ}\text{C}$ (Figure 6).

Overall, a qualitative comparison of the solution behavior of complexes with alkylamine axial donors, ($R\text{N4}$)Cu^I, indicates that the steric bulk of the alkyl group of the axial amines has a dual effect on the conformational behavior of the derived complexes: (i) increasing the steric bulk of the R substituent leads to higher preference toward the isomer with a κ^3 -bound $R\text{N4}$ ligand; (ii) increasing the steric bulk of the alkyl R groups slows down conformational exchange in these systems.

Compared to the alkylamine analogues, the Ts-substituted complex **10** undergoes much faster conformational exchange, so that slow exchange conditions could not be reached even at $-80\text{ }^{\circ}\text{C}$. This is likely due to weak coordination of the electron-deficient N–Ts group to the Cu^I center, also consistent with the significantly longer Cu^I–N bond distances observed in complex **10** compared to the alkylamine derivatives (even the ones with the bulky ^{*t*}Bu and ^{*i*}Pr groups). The ¹H NMR spectrum of **10** at $-80\text{ }^{\circ}\text{C}$ features two broadened doublets of CH₂ groups and only one signal corresponding to the meta protons of pyridines, indicative of the effective C_{2v} symmetry in solution. While this could be consistent with κ^4 (or κ^2) coordination of the ^{*Ts*}N4 ligand in solution, the high fluxionality of this complex does not allow unambiguous assignment of the conformational preference because the observed signals could also result from exchange between several configurational isomers, leading to effective averaging of the signals.

Electrochemical Properties. The electrochemical properties of cationic and neutral pyridinophane complexes were studied by CV (Figure 7). The cationic complexes were examined by CV in a MeCN solution using ^{*n*}Bu₄NPF₆ (for **1**, **3**, and **4**) and ^{*n*}Bu₄NBF₄ (for **2**) as supporting electrolytes: their electrochemical properties are summarized in Table 7. For all cationic complexes except Ts-substituted compound **4**, the chemically reversible oxidation wave assigned to a Cu^I/Cu^{II} oxidation event was observed. The separation between the forward and reverse peaks was in a range of 55–89 mV, larger than expected for an electrochemically reversible process for the majority of the complexes except the least sterically hindered

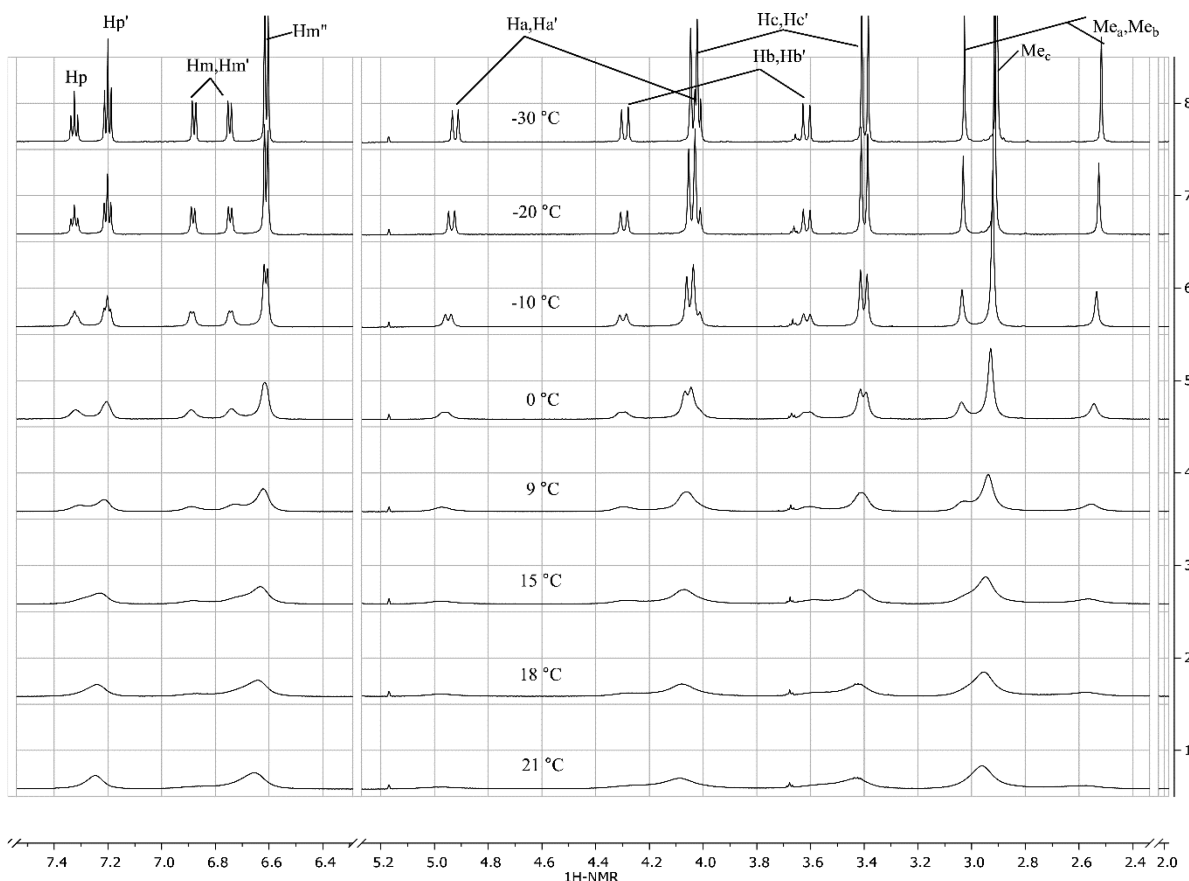


Figure 6. ^1H VT NMR spectra of complex **9** in CD_2Cl_2 .

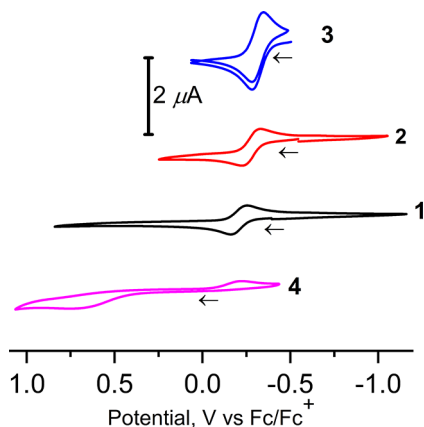


Figure 7. Cyclic voltammograms of complexes **1**, **3**, and **4** (1 mM) in 0.1 M $\text{Bu}_4\text{NPF}_6/\text{MeCN}$ and **2** in a 0.1 M $\text{Bu}_4\text{NBF}_4/\text{MeCN}$ solution at 23 °C (scan rate 100 mV s^{-1} ; 1.6 mm Pt disk working electrode; the arrow indicates the initial scan direction).

3.⁸⁶ This is likely due to significant structural changes that occur during oxidation of the pentacoordinate Cu^{I} center to form hexacoordinate Cu^{II} species. According to a literature example, a similar large separation between the anodic and cathodic peaks was observed in complex $[(^{\text{Bu}}\text{N4})\text{Cu}^{\text{I}}(\text{MeCN})]\text{X}$ ($\text{X} = \text{PF}_6$, OTf).⁶¹ In this earlier work, the oxidation product, copper(II) complex $[(^{\text{Bu}}\text{N4})\text{Cu}^{\text{II}}(\text{MeCN})_2](\text{OTf})_2$, was previously obtained and structurally characterized. Complex $[(^{\text{Bu}}\text{N4})\text{Cu}^{\text{II}}(\text{MeCN})_2](\text{OTf})_2$ featured a distorted octahedral Cu^{II} center with two MeCN ligands and with significantly shortened

Table 7. Electrochemical Properties of Complexes $[(^{\text{R}}\text{N4})\text{Cu}^{\text{I}}(\text{MeCN})]\text{X}$ (**1–4**; $\text{X} = \text{PF}_6$, BF_4)^a

complex	E_{pf}^b (mV)	E_{pr}^c (mV)	ΔE (mV) ^d	$E_{1/2}$ (mV) ^e
$[(^{\text{Pr}}\text{N4})\text{Cu}^{\text{I}}(\text{MeCN})](\text{PF}_6)$ (1)	−163	−249	89	−206
$[(^{\text{Me}}\text{N4})\text{Cu}^{\text{I}}(\text{MeCN})](\text{BF}_4)$ (2) ^f	−241	−316	75	−279
$[(^{\text{H}}\text{N4})\text{Cu}^{\text{I}}(\text{MeCN})](\text{PF}_6)$ (3)	−289	−344	55	−317
$[(^{\text{Ts}}\text{N4})\text{Cu}^{\text{I}}(\text{MeCN})](\text{PF}_6)$ (4) ^g	674	−205		

^aCyclic voltammograms for complexes **1–4** (1 mM) in a 0.1 M solution of Bu_4NPF_6 (for **1**, **3**, and **4**) or Bu_4NBF_4 (for **2**) as supporting electrolytes in MeCN at 23 °C [100 mV s^{-1} scan rate; Pt disk electrode ($d = 1.6$ mm); all peaks were referenced versus ferrocene]. ^bPotential of the forward peak. ^cPotential of the return peak. ^dThe peak-to-peak separation ΔE was calculated as $E_{\text{pf}} - E_{\text{pr}}$. ^e $E_{1/2}$ was estimated as $1/2(E_{\text{pf}} + E_{\text{pr}})$. ^f Bu_4NBF_4 was used as an electrolyte. ^gIrreversible oxidation.

Cu–axial amine bond distances compared to its copper(I) analogue $[(^{\text{Bu}}\text{N4})\text{Cu}^{\text{I}}(\text{MeCN})](\text{OTf})$.⁶¹

Interestingly, the estimated $E_{1/2}$ of the $\text{Cu}^{\text{I}}/\text{Cu}^{\text{II}}$ oxidation wave varies depending on the substituents at the amine axial donors, with the most positive $E_{1/2}$ being observed for the complex with the bulkiest $^{\text{Pr}}$ substituent, **1**, and most negative $E_{1/2}$ observed for the least sterically hindered complex **3**. This trend is different from what could have been expected based solely on the donor properties of the axial amines, and it likely reflects the degree of stabilization of the copper(II) product due

to differences in the steric bulk of the axial donor. Because significantly shorter Cu–N_{amine} bond distances are expected for the oxidized copper(II) complex, more effective stabilization is expected from the least bulky ligands.

Compared to complexes 1–3, the Ts-substituted complex 4 featured an irreversible oxidation wave at a much higher potential, which could be a result of the poor stability of the copper(II) product in the presence of weakly coordinating axial NTs groups.

Compared to cationic complexes, the electrochemical behavior of neutral copper(I) iodide complexes (^RN4)CuI (5–10) is generally more complex and is likely affected by the redox activity of a free iodide ion that can be released into solution in the presence of an electrolyte, which prevented us from carrying out detailed electrochemical studies on the copper iodide complex series.⁷¹

Photophysical Properties. The UV–vis absorption spectra of complexes 1–4 in a MeCN solution and complexes 5–10 in dichloromethane were recorded (Figure 8). All complexes feature an intense absorption band at 230–300 nm assigned as the ligand-centered transition. Similarly, free pyridinophane ligands also show an absorption band in this region.⁶⁰ R₄N4-supported complexes 1–3 and 5–9, where R = H,

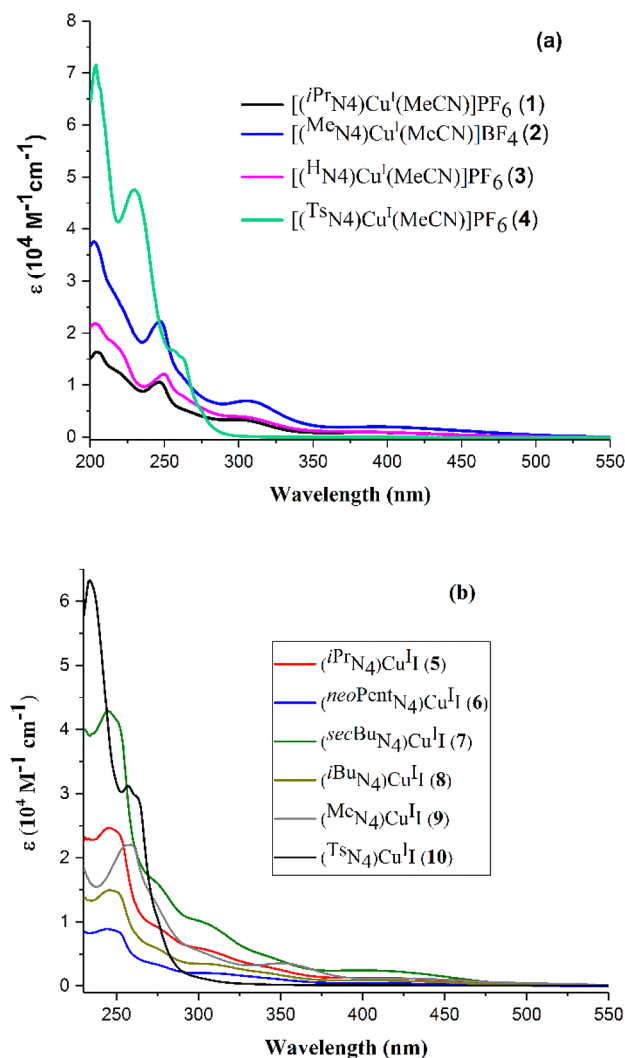


Figure 8. UV–vis absorbance spectra for complexes 1–4 in MeCN (a) and 5–10 in dichloromethane (b).

Me, ⁱBu, ^{sec}Bu, ^{neo}Pent, and ⁱPr, are also characterized by a less intense metal-to-ligand charge-transfer (MLCT) band ($\epsilon \approx 10^4 \text{ M}^{-1} \text{ cm}^{-1}$) at 390–430 nm (Table 9). By contrast to complexes with alkyl-substituted pyridinophane ligands, the Ts-substituted analogues 4 and 10 did not exhibit any absorption bands above 300 nm.

The emission properties of the cationic and neutral complexes were then studied in the solid state and in solution to elucidate interplay between the ligand steric and photophysical properties of copper(I) complexes in a series containing ⁱBu, ⁱPr, ^{neo}Pent, ^{sec}Bu, ⁱBu, and Me substituents at the amine. While the cationic MeCN complexes 1–4 showed negligible emission in the solid state upon excitation at 400 nm (typically <5%), the neutral copper(I) iodide complexes 5–9 bearing alkyl substituents at the amine donors exhibited broad emission bands with the maximum in the range of 540–589 nm at 298 K, indicative of the charge-transfer character of the emissive excited states^{49,54,57,87} and consistent with previously reported time-dependent density functional theory studies (Figure 9).⁶⁰ The photophysical

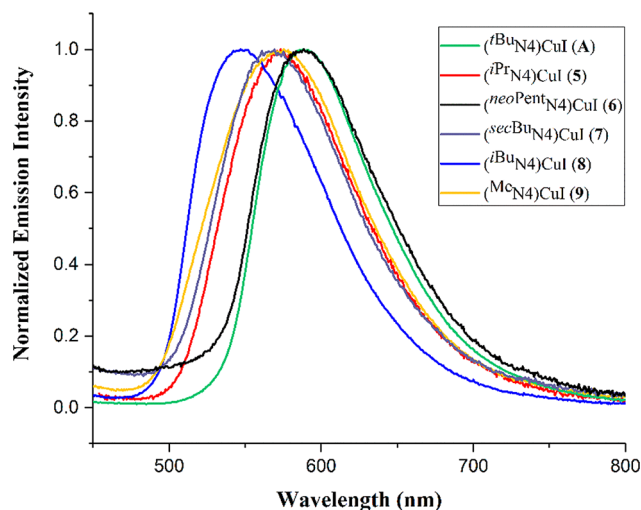


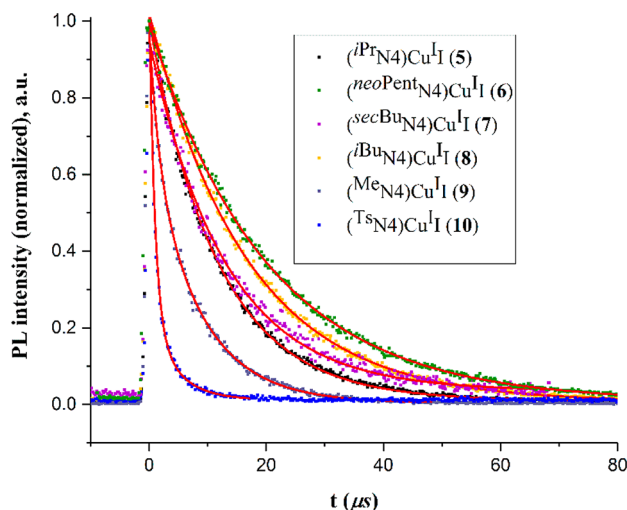
Figure 9. Normalized emission spectra of complexes A and 5–9 in the solid state at 298 K. Excitation at 400 nm.

properties of complexes 5–9 as well as a comparison with the previously reported complex A at room temperature are summarized in Table 8. In all cases, the average emission lifetimes were in the microsecond range, varying from 6.3 to 20.02 μs , indicating phosphorescence from the triplet excited state (Figure 10), although thermally activated delayed fluorescence (TADF) cannot be completely excluded.^{60,88} Complex 9 showed only negligible emission (<3%) under the same conditions. The emission decay profile could be fit with a monoexponential curve, except for complex 9, in which a biexponential fit gave two components with lifetimes of 1.70 and 8.39 μs , with an intensity-weighted average value of 6.31 μs .

A comparison of the PLQYs in Table 8 shows that the highest PLQY was observed for the most bulky ⁱBu-substituted complex A, while the least sterically hindered complex 9 showed the lowest PLQY. Accordingly, the nonradiative decay rate constant k_{nr} was lowest for complex A ($1.39 \times 10^4 \text{ s}^{-1}$) and highest for complex 9 ($15.68 \times 10^4 \text{ s}^{-1}$) in this series. Complexes with intermediate steric hindrance at the axial amines, 5–8, exhibit PLQYs in the range of 0.39–0.55 with k_{nr} falling in the intermediate range [$(2.25\text{--}4.65) \times 10^4 \text{ s}^{-1}$].

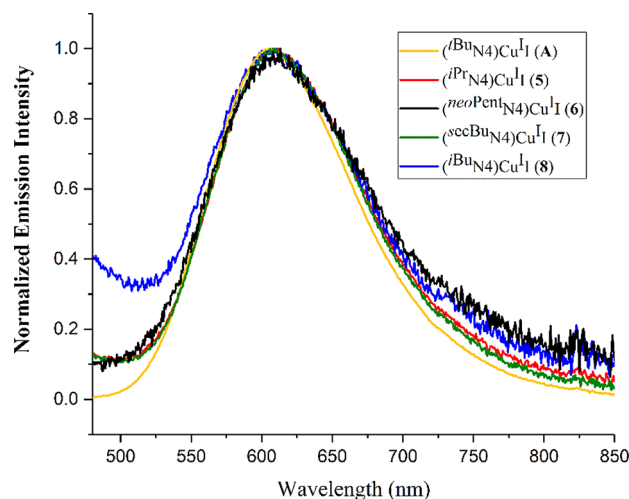
Table 8. Photophysical Properties of Complexes 5–9 and A in the Solid State at 298 K^a

complex	λ_{em}^b (nm)	Φ^c	τ (μs) ^d	$k_r \times 10^{-4}$ (s ⁻¹) ^e	$k_{\text{nr}} \times 10^{-4}$ (s ⁻¹) ^f	CIE color coordinates (x, y) ^g
(^t BuN4)Cu ^I (A) ^h	585	0.78	15.79	4.94	1.39	0.514, 0.476
(ⁱ PrN4)Cu ^I (5)	576	0.58	11.66	4.97	3.59	0.487, 0.506
(^{neo} PentN4)Cu ^I (6)	589	0.55	20.02	2.75	2.25	0.549, 0.439
(^{sec} BuN4)Cu ^I (7)	570	0.40	12.96	3.10	4.65	0.323, 0.268
(^t BuN4)Cu ^I (8)	546	0.39	16.69	2.34	3.66	0.414, 0.562
(MeN4)Cu ^I (9)	570	0.02	6.31 ⁱ	0.32	15.68	0.470, 0.512

^aAll measurements were performed with excitation at 400 nm.^bEmission maximum. ^cPLQYs at 298 K (excitation at 400 nm).^dEmission lifetime at 298 K. ^eRadiative decay rate constants were estimated as Φ/τ . ^fNonradiative decay rate constants were calculated as $k_r(1 - \Phi)/\Phi$. ^gCIE 1931 chromaticity diagram coordinates. ^hFrom ref 60. ⁱIntensity-weighted average value based on a biexponential fit (calculated from $\alpha_1\tau_1 + \alpha_2\tau_2/(\alpha_1 + \alpha_2)$, where $\tau_1 = 1.70$ and $\tau_2 = 8.39$ are the decay components and $\alpha_1 = (A_1/A_1 + A_2)$ and $\alpha_2 = (A_2/A_1 + A_2)$ are the respective amplitudes, where $A_1 = 0.301$ and $A_2 = 0.668$ are the respective contributions).**Figure 10.** Normalized PL decay profiles for complexes 5–10 (500–800 nm range) in the solid state at 298 K. Excitation at 400 nm.

To exclude the effects of crystal packing and aggregation on the photophysical properties, we examined the emission properties in solution at 298 K and in a frozen solution at 77 K. To our satisfaction, solutions of complexes bearing ⁱPrN4 (5), ^{neo}PentN4 (6), ^{sec}BuN4 (7), and ^tBuN4 (8) in CH₂Cl₂ at 298 K showed emission at 600–615 nm (Figure 11), and only the complex with the least bulky Me group (9) showed negligible emission with PLQY < 0.01. In polar-coordinating solvents such as alcohols or nitriles, the emission was negligible, while low solubility prevented measurements in benzene and toluene solutions. A comparison of the CH₂Cl₂ solution PLQY data for 5–9 and A shows that the PLQY gradually decreases in the order ^tBu > ⁱPr ≈ ^{sec}Bu > ^{neo}Pent > Me (Table 9), thus showing a clear correlation with the steric bulk.^{89–92}

Compared to the solid state, the emission lifetimes at 298 K are significantly shorter, falling to a 0.7–6 μs range (Figure 12).

**Figure 11.** Normalized emission spectra of complexes A and 5–8 in a CH₂Cl₂ solution at 298 K. Excitation at 400 nm.

While the radiative rate constants remain in a range similar to that in the solid state, the solution-state k_{nr} increases by about an order of magnitude, indicative of faster nonradiative decay pathways in the solutions of conformationally flexible complexes (^RN4)Cu^I. Complex 10 showed only negligible emission in the solid state (PLQY < 0.01) and was not emissive in solution (vide infra) as well as a different electronic structure consistent with the lack of MLCT bands at ca. 400 nm; variation of the excitation source wavelength to higher energies also did not result in any observable emission. In particular, conformation of the ^{Ts}N4 ligand in complex 10 in solution can differ from other alkyl-substituted complexes, although solution NMR studies did not allow us to unambiguously confirm the conformational assignment because of the high fluxionality of this complex (vide supra).

The frozen MeTHF solutions of complexes A and 5–10 at 77 K show a dramatic increase of the PLQY compared to RT measurements, reaching 0.79–0.91 for complexes (^RN4)Cu^I (R = ^tBu, ⁱPr, ^{neo}Pent, ^{sec}Bu, ^tBu) and 0.25 for 9, which was nonemissive at RT (Figure 13). This resembles the behavior of 2,9-disubstituted bis(phenanthroline)copper(I) complexes with long-alkyl-chain substituents in frozen solutions, which was attributed to the ability of long alkyl chains to prevent significant distortions of the ground and excited states in a rigid matrix.⁹³

The observed correlation between the steric bulk of the amine donor and the PLQY could be affected by two main factors. First, as shown by the NMR studies, the steric bulk of the alkyl group affected the rate of the conformational exchange processes in solutions of (^RN4)Cu^I (including degenerative exchange), with slower conformational exchange observed for the complexes bearing the more bulky alkyl groups at the amines (vide supra). Second, the steric bulk of the alkyl group also affected the relative stabilities of two different isomers in solution, with tetracoordinate (κ^3 -^RN4)Cu^I species being more favorable for more sterically demanding R groups. However, in the case of complexes A, 6, and 8, only one conformer, (κ^3 -^RN4)Cu^I, was present in solution in both cases, while the solution quantum yield decreased drastically for less bulky and more fluxional complexes 6 and 8 compared to ^tBu-substituted complex A, showing that the fluxionality may be the predominant factor affecting the solution PLQY.

Table 9. Photophysical Properties of Complexes 5–10 and A in Solution^a

complex	λ_{abs} (nm) ^b [ϵ (M ⁻¹ cm ⁻¹) ^c	298 K ^d		77 K ^e		τ (μ s) ^h	$k_r \times 10^{-4}$ (s ⁻¹) ⁱ	$k_{\text{nr}} \times 10^{-5}$ (s ⁻¹) ^j	CIE color coordinates (x, y) ^k
		λ_{emi} (nm) ^e	Φ^f	λ_{emi} (nm) ^e	Φ^f				
(^t BuN4)CuI (A) ^l	419 [2031]	600	0.28	568	0.81	4.3	6.51	1.67	0.372, 0.245
(ⁱ PrN4)CuI (5)	415 [1190]	612	0.095	572	0.79	6.17	1.54	1.47	0.388, 0.252
(^{neo} PentN4)CuI (6)	434 [345]	613	0.025	567	0.91	0.70	3.57	13.9	0.377, 0.242
(^{sec} BuN4)CuI (7)	407 [2380]	609	0.11	575	0.72	3.34	3.29	2.66	0.389, 0.258
(^t BuN4)CuI (8)	417 [811]	610	0.059	559	0.79	2.16	2.73	4.35	0.261, 0.126
(MeN4)CuI (9)	432 [1090]	n.d.	<0.01	571	0.25	n.d.	n.d.	n.d.	n.d.
(^t SuN4)CuI (10)	n.d.	n.d.	<0.01	499	0.53	n.d.	n.d.	n.d.	n.d.

^aAll measurements were performed with excitation at 400 nm; n.d. = not determined. ^bAbsorption maximum. ^cExtinction coefficient. ^dIn degassed dichloromethane at 298 K. ^eEmission maximum. ^fPLQY. ^gIn MeTHF at 77 K. ^hEmission lifetime at 298 K in CH₂Cl₂. ⁱRadiative decay rate constants were estimated as Φ/τ ; measured at 298 K in CH₂Cl₂. ^jNonradiative decay rate constants were calculated as $k_r(1 - \Phi)/\Phi$; measured at 298 K in CH₂Cl₂. ^kCIE 1931 chromaticity diagram coordinates determined for the emission spectrum at 298 K in CH₂Cl₂. ^lFrom ref 60.

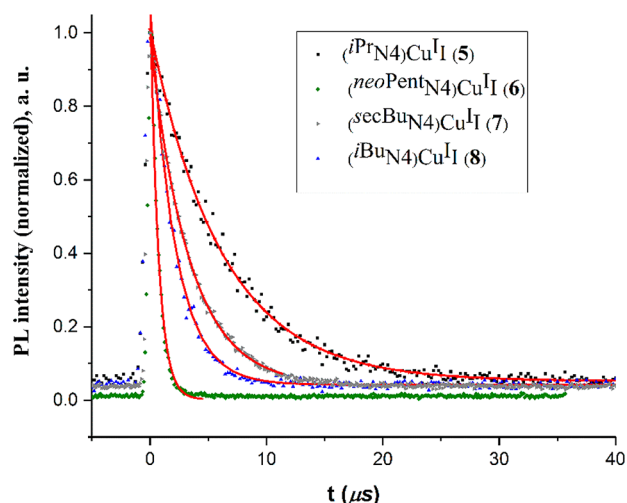


Figure 12. Normalized PL decay profiles for copper iodide complexes 5–8 (500–800 nm range) in a CH₂Cl₂ solution at 298 K. Excitation at 400 nm.

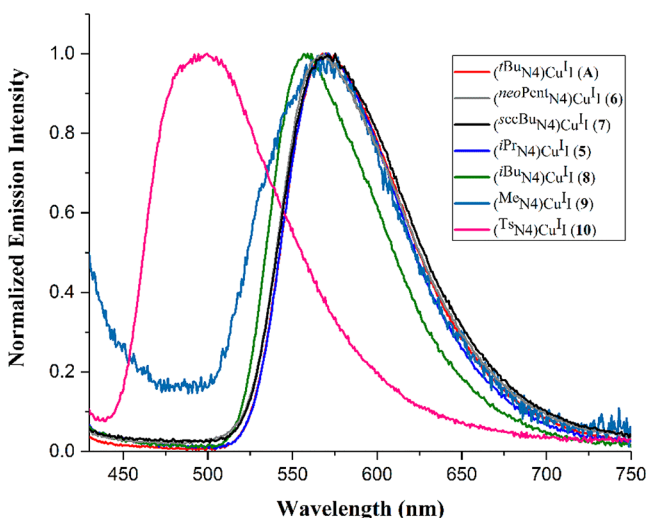


Figure 13. Normalized emission spectra of complexes A and 5–10 in frozen MeTHF at 77 K. Excitation at 400 nm.

Similarly, the effect of the ligand steric bulk on the photophysical properties was described for a series of copper(I) complexes with phenanthroline-based ligands Cu(NN)₂⁺ and Cu(NN)(PP) (NN = substituted phenanthroline; PP =

diphosphine). Introducing bulky substituents at the phenanthroline backbone leads to a significant increase in the emission lifetime and PLQY. The detailed investigations of these systems showed that such a strong effect of the ligand steric properties arises because of suppression of the flattening distortion in the charge-transfer state, thus preventing nonradiative structural relaxation.^{30,37,51,56,94–96} Although the geometrical changes involved in nonradiative relaxation may differ, suppression of the ligand dynamics achieved by introducing bulky substituents at the weakly interacting amine donors in (^RN4)CuI complexes is also the main factor that determines the PLQY in this series. Although the ligand dynamic process observed by NMR involving degenerative exchange between two axial amines is much slower than the nonradiative decay, the introduction of the steric bulk at amine substituents might affect the fluxionality of the ligand in the excited state in a similar manner. In addition, dynamic processes in the excited state might feature faster rate constants because of charge buildup at the Cu center and at the pyridinophane ligand.⁶⁰

In addition, it has been reported that, in the case of tetracoordinate complex [Cu^I(dmp)₂]⁺ (dmp = 2,9-dimethyl-1,10-phenanthroline), coordination of a Lewis basic solvent such as MeCN to the MLCT excited state leads to “exciplex” quenching.^{38,51,64,65} In the present (^RN4)CuI system, the free axial amine moiety can coordinate to the Cu center in the absence of coordinating solvents. Thus, suppression of the nucleophilic attack by the pendant amine donor to the Cu center in the excited state due to the presence of bulky alkyl substituents could be another mechanism responsible for the higher PLQY observed for complexes with bulky substituents at the amine donors. A higher propensity of complexes with less bulky substituents to undergo pendant amine donor coordination is observed in the solution behavior of (^RN4)CuI studied by NMR, which shows that only 9 exhibits a substantial fraction of a pentacoordinate [(^κ⁴-^RN4)CuI], and isomer interconversion is faster compared to that of the ^tBu- and ⁱPr-substituted analogues. Moreover, the trend in the oxidation potentials of pentacoordinate complexes 1–4 also confirms that stabilization of a Cu^{II} center is favored by less bulky amine donors because of the more efficient coordination of the axial amines (vide supra).

Interestingly, the PLQYs in frozen solutions for ^tBu-, ⁱPr-, ^{neo}Pent-, ^{sec}Bu-, and ^tBu-substituted complexes are very similar, 0.72–0.91, while the Me-substituted complex 9 shows a lower PLQY of 0.25. Similarly, Armaroli and co-workers reported high emission intensity in frozen solution 2,9-disubstituted bis-(phenanthroline)copper(I) complexes with long-alkyl-chain

substituents.⁹³ At the same time, the Me-substituted bis-(phenanthroline)copper(I) complex remained a weak emitter in a frozen solution, and it was proposed that smaller Me substituents do not prevent excited-state distortions even in a rigid matrix. By analogy, one could propose that at 77 K conformational exchange and nucleophilic attack by pendant amine are essentially “frozen”, and therefore no significant differentiation of the PLQY is observed for complexes (^RN4)Cu^I (R = ^tBu, ⁱPr, ^{neo}Pent, ^{sec}Bu, ⁱBu), all containing bulky alkyl groups that can effectively prevent distortions in the excited state, leading to leveling off the PLQY to similarly high values of 0.72–0.91. Interestingly, even Ts-substituted complex **10**, which was highly fluxional in solution at RT, becomes emissive in a frozen solution with a PLQY of 0.53, which further confirms the importance of “freezing” the conformational lability for emissive properties.

Overall, although the Cu–N_{amine} distances are significantly longer than the Cu–N_{pyridine} distances, the emissive properties of complexes **5–9** are very sensitive to steric requirements of the axial amine arms, which determine the dynamic properties of the macrocyclic pyridinophane ligand. Such sensitivity to subtle changes at the axial amine environment and its effect on the ligand fluxionality are likely the key features that enabled the use of analogous, covalently copolymerized complexes as emissive probes for detecting stress in polymer films.

CONCLUSION

In summary, we have explored in detail the structure, ligand conformational behavior, and redox and photophysical properties of a series of copper(I) complexes with a conformationally fluxional ^RN4 pyridinophane ligand. Steric requirements of the axial amine substituents in these complexes were shown to play a key role in determining the solution behavior and emissive properties of these complexes. The solution NMR studies revealed two types of exchange processes that exist in solutions of (^RN4)Cu^I, one involving degenerative exchange between two axial amino groups in a κ^3 -coordinated ligand and another being the exchange between the κ^3 - and κ^4 -bound ligand isomers. The dynamics of exchange were directly correlated to the steric bulk of the alkyl group at the amines, with complexes containing more bulky alkyl groups at the amines showing slower conformational exchange.

Moreover, we have shown that the mononuclear complexes supported by an N-donor macrocyclic ligand, (^RN4)Cu^I, show emissive properties in solution and in the solid state, with the PLQY highly sensitive to the steric bulk of the amine substituents, likely through suppression of the nonradiative decay pathways in less fluxional complexes bearing bulkier alkyl groups. Because the steric bulk of the alkyl group at the amine can be easily controlled by simple synthetic modifications, this offers a convenient strategy for control of the photophysical properties of simple, solution-stable mononuclear copper(I) complexes. Importantly, the current study showed that, although increasing the steric bulk effects the axial amine–Cu^I center distance, it does not lead to faster exchange equilibria, and the quantum yield and emission lifetime only improve in the series of simple alkyl-substituted complexes studied here. These photophysical properties are adversely affected when an alkyl group is substituted for an electron-withdrawing Ts moiety. These findings have a direct implication in the design of future dynamic polymer probes,⁶⁶ where we will seek to introduce even bulkier, alkyl-based substituents in order to decrease the amount

of organometallic comonomer required for visual observation of the mechanical stress.

ASSOCIATED CONTENT

Supporting Information

The Supporting Information is available free of charge on the ACS Publications website at DOI: 10.1021/acs.inorgchem.8b01181.

Synthesis, characterization, and full NMR, UV–vis, and FT-IR spectra of complexes **1–10**, spin-saturation transfer kinetic experiments, cyclic voltammograms of complexes **5–10**, and X-ray structure determination details (PDF)

Accession Codes

CCDC 1818217–1818224 and 1851237–1851238 contain the supplementary crystallographic data for this paper. These data can be obtained free of charge via www.ccdc.cam.ac.uk/data_request/cif, or by emailing data_request@ccdc.cam.ac.uk, or by contacting The Cambridge Crystallographic Data Centre, 12 Union Road, Cambridge CB2 1EZ, UK; fax: +44 1223 336033.

AUTHOR INFORMATION

Corresponding Author

*E-mail: juliak@oist.jp (J.R.K.).

ORCID

Robert R. Fayzullin: 0000-0002-3740-9833

Julia R. Khusnutdinova: 0000-0002-5911-4382

Notes

The authors declare no competing financial interest.

ACKNOWLEDGMENTS

We thank Dr. Hirohiko Watanabe (Hamamatsu Photonics) for kind assistance with measurement of the PLQYs and Dr. Kieran Deasy (Mechanical Engineering & Microfabrication support section, OIST) for help with the emission lifetime measurements, and special thanks go to Dr. Michael Roy (technical support for NMR, mass spectrometry, and elemental analysis). We are also sincerely grateful to Dr. Pavlos Stampoulis (JEOL RESONANCE Inc.) and Prof. Ilya Gridnev (Tohoku University) for discussions and suggestions regarding NMR measurements. We also thank Dr. Ayumu Karimata and Dr. Nancy Singhal for helpful discussions. The authors acknowledge the Okinawa Institute of Science and Technology Graduate University for start-up funding. This work was supported by JSPS KAKENHI Grant JP18K05247.

REFERENCES

- (1) Chang-Yen, D. A.; Lvov, Y.; McShane, M. J.; Gale, B. K. Electrostatic Self-Assembly of a Ruthenium-Based Oxygen Sensitive Dye Using Polyion–Dye Interpolyelectrolyte Formation. *Sens. Actuators, B* **2002**, *87*, 336–345.
- (2) Cooke, M. W.; Hanan, G. S. Luminescent Polynuclear Assemblies. *Chem. Soc. Rev.* **2007**, *36*, 1466–1476.
- (3) Du, P.; Schneider, J.; Brennessel, W. W.; Eisenberg, R. Synthesis and Structural Characterization of a New Vapochromic Pt(II) Complex Based on the 1-Terpyridyl-2,3,4,5,6-Pentaphenylbenzene (Tpppb) Ligand. *Inorg. Chem.* **2008**, *47*, 69–77.
- (4) Gong, X.; Robinson, M. R.; Ostrowski, J. C.; Moses, D.; Bazan, G. C.; Heeger, A. J. High-Efficiency Polymer-Based Electrophosphorescent Devices. *Adv. Mater.* **2002**, *14*, 581–585.

- (5) Islam, A.; Sugihara, H.; Arakawa, H. Molecular Design of Ruthenium(II) Polypyridyl Photosensitizers for Efficient Nanocrystalline TiO₂ Solar Cells. *J. Photochem. Photobiol., A* **2003**, *158*, 131–138.
- (6) Kalyanasundaram, K.; Grätzel, M. Applications of Functionalized Transition Metal Complexes in Photonic and Optoelectronic Devices. *Coord. Chem. Rev.* **1998**, *177*, 347–414.
- (7) Keefe, M. H.; Benkstein, K. D.; Hupp, J. T. Luminescent Sensor Molecules Based on Coordinated Metals: A Review of Recent Developments. *Coord. Chem. Rev.* **2000**, *205*, 201–228.
- (8) Köhler, A.; Wilson, J. S.; Friend, R. H. Fluorescence and Phosphorescence in Organic Materials. *Adv. Mater.* **2002**, *14*, 701–707.
- (9) Mukherjee, S.; Thilagar, P. Recent Advances in Purely Organic Phosphorescent Materials. *Chem. Commun.* **2015**, *51*, 10988–11003.
- (10) Muller, G. Luminescent Chiral Lanthanide(III) Complexes as Potential Molecular Probes. *Dalton Trans.* **2009**, 9692–9707.
- (11) Ohara, H.; Ogawa, T.; Yoshida, M.; Kobayashi, A.; Kato, M. Reversible Luminescent Colour Changes of Mononuclear Copper(I) Complexes Based on Ligand Exchange Reactions by N-Heteroaromatic Vapours. *Dalton Trans.* **2017**, *46*, 3755–3760.
- (12) Ramdass, A.; Sathish, V.; Velayudham, M.; Thanasekaran, P.; Umaphathy, S.; Rajagopal, S. Luminescent Sensor for Copper(II) Ion Based on Imine Functionalized Monometallic Rhenium(I) Complexes. *Sens. Actuators, B* **2017**, *240*, 1216–1225.
- (13) Sakaki, S.; Kuroki, T.; Hamada, T. Synthesis of a New Copper(I) Complex, [Cu(Tmdcbpy)]⁺ (Tmdcbpy = 4,4',6,6'-Tetramethyl-2,2'-Bipyridine-5,5'-Dicarboxylic Acid), and Its Application to Solar Cells. *J. Chem. Soc., Dalton Trans.* **2002**, 840–842.
- (14) Wei, W.; Wu, M.; Gao, Q.; Zhang, Q.; Huang, Y.; Jiang, F.; Hong, M. A Novel Supramolecular Tetrahedron Assembled from Tetranuclear Copper(I) Cluster Molecules Via Aryl Embrace Interactions. *Inorg. Chem.* **2009**, *48*, 420–422.
- (15) Xiang, H.; Cheng, J.; Ma, X.; Zhou, X.; Chruma, J. J. Near-Infrared Phosphorescence: Materials and Applications. *Chem. Soc. Rev.* **2013**, *42*, 6128–6185.
- (16) Yook, K. S.; Lee, J. Y. Organic Materials for Deep Blue Phosphorescent Organic Light-Emitting Diodes. *Adv. Mater.* **2012**, *24*, 3169–3190.
- (17) Zhang, Q.; Zhou, Q.; Cheng, Y.; Wang, L.; Ma, D.; Jing, X.; Wang, F. Highly Efficient Green Phosphorescent Organic Light-Emitting Diodes Based on Cu^I Complexes. *Adv. Mater.* **2004**, *16*, 432–436.
- (18) Che, C. M.; Kwok, C. C.; Lai, S. W.; Rausch, A. F.; Finkenzeller, W. J.; Zhu, N.; Yersin, H. Photophysical Properties and OLED Applications of Phosphorescent Platinum(II) Schiff Base Complexes. *Chem. - Eur. J.* **2010**, *16*, 233–247.
- (19) Del Guerzo, A.; Leroy, S.; Fages, F.; Schmehl, R. H. Photophysics of Re(I) and Ru(II) Diimine Complexes Covalently Linked to Pyrene: Contributions from Intra-Ligand Charge Transfer States. *Inorg. Chem.* **2002**, *41*, 359–366.
- (20) Fleetham, T.; Li, G.; Li, J. Phosphorescent Pt(II) and Pd(II) Complexes for Efficient, High-Color-Quality, and Stable OLEDs. *Adv. Mater.* **2017**, *29*, 1601861–1601876.
- (21) He, L.; Qiao, J.; Duan, L.; Dong, G.; Zhang, D.; Wang, L.; Qiu, Y. Toward Highly Efficient Solid-State White Light-Emitting Electrochemical Cells: Blue-Green to Red Emitting Cationic Iridium Complexes with Imidazole-Type Ancillary Ligands. *Adv. Funct. Mater.* **2009**, *19*, 2950–2960.
- (22) Lowry, M. S.; Bernhard, S. Synthetically Tailored Excited States: Phosphorescent, Cyclometalated Iridium(III) Complexes and Their Applications. *Chem. - Eur. J.* **2006**, *12*, 7970–7977.
- (23) Rausch, A. F.; Murphy, L.; Williams, J. A.; Yersin, H. Improving the Performance of Pt(II) Complexes for Blue Light Emission by Enhancing the Molecular Rigidity. *Inorg. Chem.* **2012**, *51*, 312–319.
- (24) Tsuzuki, T.; Tokito, S. Highly Efficient and Low-Voltage Phosphorescent Organic Light-Emitting Diodes Using an Iridium Complex as the Host Material. *Adv. Mater.* **2007**, *19*, 276–280.
- (25) Tung, Y. L.; Lee, S. W.; Chi, Y.; Chen, L. S.; Shu, C. F.; Wu, F. I.; Carty, A. J.; Chou, P. T.; Peng, S. M.; Lee, G. H. Organic Light-Emitting Diodes Based on Charge-Neutral Ru^{II} Phosphorescent Emitters. *Adv. Mater.* **2005**, *17*, 1059–1064.
- (26) Ulbricht, C.; Beyer, B.; Friebe, C.; Winter, A.; Schubert, U. S. Recent Developments in the Application of Phosphorescent Iridium(III) Complex Systems. *Adv. Mater.* **2009**, *21*, 4418–4441.
- (27) Wong, W.-Y.; He, Z.; So, S.-K.; Tong, K.-L.; Lin, Z. A Multifunctional Platinum-Based Triplet Emitter for OLED Applications. *Organometallics* **2005**, *24*, 4079–4082.
- (28) Yang, C. H.; Cheng, Y. M.; Chi, Y.; Hsu, C. J.; Fang, F. C.; Wong, K. T.; Chou, P. T.; Chang, C. H.; Tsai, M. H.; Wu, C. C. Blue-Emitting Heteroleptic Iridium(III) Complexes Suitable for High-Efficiency Phosphorescent OLEDs. *Angew. Chem., Int. Ed.* **2007**, *46*, 2418–2421.
- (29) Zhang, Y.; Liu, Z.; Yang, K.; Zhang, Y.; Xu, Y.; Li, H.; Wang, C.; Lu, A.; Sun, S. A Ruthenium(II) Complex as Turn-on Cu(II) Luminescent Sensor Based on Oxidative Cyclization Mechanism and Its Application in Vivo. *Sci. Rep.* **2015**, *5*, 8172–8176.
- (30) Barbieri, A.; Accorsi, G.; Armaroli, N. Luminescent Complexes Beyond the Platinum Group: The d¹⁰ Avenue. *Chem. Commun.* **2008**, 2185–2193.
- (31) Czerwieniec, R.; Hofbeck, T.; Crespo, O.; Laguna, A.; Concepcion Gimeno, M.; Yersin, H. The Lowest Excited State of Brightly Emitting Gold(I) Triphosphine Complexes. *Inorg. Chem.* **2010**, *49*, 3764–3767.
- (32) Ford, P. C.; Cariati, E.; Bourassa, J. Photoluminescence Properties of Multinuclear Copper(I) Compounds. *Chem. Rev.* **1999**, *99*, 3625–3648.
- (33) Hsu, C. W.; Lin, C. C.; Chung, M. W.; Chi, Y.; Lee, G. H.; Chou, P. T.; Chang, C. H.; Chen, P. Y. Systematic Investigation of the Metal-Structure-Photophysics Relationship of Emissive d¹⁰-Complexes of Group 11 Elements: The Prospect of Application in Organic Light Emitting Devices. *J. Am. Chem. Soc.* **2011**, *133*, 12085–12099.
- (34) Liu, Z.; Qiu, J.; Wei, F.; Wang, J.; Liu, X.; Helander, M. G.; Rodney, S.; Wang, Z.; Bian, Z.; Lu, Z.; Thompson, M. E.; Huang, C. Simple and High Efficiency Phosphorescence Organic Light-Emitting Diodes with Codeposited Copper(I) Emitter. *Chem. Mater.* **2014**, *26*, 2368–2373.
- (35) Matsumoto, K.; Shindo, T.; Mukasa, N.; Tsukuda, T.; Tsubomura, T. Luminescent Mononuclear Ag(I)-Bis(Diphosphine) Complexes: Correlation between the Photophysics and the Structures of Mononuclear Ag(I)-Bis(Diphosphine) Complexes. *Inorg. Chem.* **2010**, *49*, 805–814.
- (36) Yam, V. W.-W.; Lo, K. K.-W. Luminescent Polynuclear d¹⁰ Metal Complexes. *Chem. Soc. Rev.* **1999**, *28*, 323–334.
- (37) Lavie-Cambot, A. I.; Cantuel, M.; Leydet, Y.; Jonusauskas, G.; Bassani, D. M.; McClenaghan, N. D. Improving the Photophysical Properties of Copper(I) Bis(Phenanthroline) Complexes. *Coord. Chem. Rev.* **2008**, *252*, 2572–2584.
- (38) Armaroli, N.; Accorsi, G.; Cardinali, F.; Listorti, A. *Photochemistry and Photophysics of Coordination Compounds I*; Springer: Berlin, 2007; Vol. 280.
- (39) Horváth, O. Photochemistry of Copper(I) Complexes. *Coord. Chem. Rev.* **1994**, *135*–136, 303–324.
- (40) Nishikawa, M.; Sano, T.; Washimi, M.; Takao, K.; Tsubomura, T. Emission Properties and Cu(I)-Cu(I) Interaction in 2-Coordinate Dicopper(I)-Bis(N-Heterocyclic)Carbene Complexes. *Dalton Trans.* **2016**, *45*, 12127–12136.
- (41) Hofbeck, T.; Monkowius, U.; Yersin, H. Highly Efficient Luminescence of Cu(I) Compounds: Thermally Activated Delayed Fluorescence Combined with Short-Lived Phosphorescence. *J. Am. Chem. Soc.* **2015**, *137*, 399–404.
- (42) Nishikawa, M.; Wakita, Y.; Nishi, T.; Miura, T.; Tsubomura, T. Long-Lived and Oxygen-Responsive Photoluminescence in the Solid State of Copper(I) Complexes Bearing Fluorinated Diphosphine and Bipyridine Ligands. *Dalton Trans.* **2015**, *44*, 9170–9181.
- (43) Marion, R.; Sguerra, F.; Di Meo, F.; Sauvageot, E.; Lohier, J.-F.; Daniellou, R.; Renaud, J.-L.; Linares, M.; Hamel, M.; Gaillard, S. NHC Copper(I) Complexes Bearing Dipyrindylamine Ligands: Synthesis, Structural, and Photoluminescent Studies. *Inorg. Chem.* **2014**, *53*, 9181–9191.

- (44) Bizzarri, C.; Strabler, C.; Prock, J.; Trettenbrein, B.; Ruggenthaler, M.; Yang, C.-H.; Polo, F.; Iordache, A.; Briggeller, P.; Cola, L. D. Luminescent Dinuclear Cu(I) Complexes Containing Rigid Tetraphosphine Ligands. *Inorg. Chem.* **2014**, *53*, 10944–10951.
- (45) Krylova, V. A.; Djurovich, P. I.; Aronson, J. W.; Haiges, R.; Whited, M. T.; Thompson, M. E. Structural and Photophysical Studies of Phosphorescent Three-Coordinate Copper(I) Complexes Supported by an N-Heterocyclic Carbene Ligand. *Organometallics* **2012**, *31*, 7983–7993.
- (46) Krylova, V. A.; Djurovich, P. I.; Whited, M. T.; Thompson, M. E. Synthesis and Characterization of Phosphorescent Three-Coordinate Cu(I)-NHC Complexes. *Chem. Commun.* **2010**, *46*, 6696–6698.
- (47) Lotito, K. J.; Peters, J. C. Efficient Luminescence from Easily Prepared Three-Coordinate Copper(I) Arylamidophosphines. *Chem. Commun.* **2010**, *46*, 3690–3692.
- (48) Miller, A. J. M.; Dempsey, J. L.; Peters, J. C. Long-Lived and Efficient Emission from Mononuclear Amidophosphine Complexes of Copper. *Inorg. Chem.* **2007**, *46*, 7244–7246.
- (49) Tsuboyama, A.; Kuge, K.; Furugori, M.; Okada, S.; Hoshino, M.; Ueno, K. Photophysical Properties of Highly Luminescent Copper(I) Halide Complexes Chelated with 1,2-Bis(Diphenylphosphino)-Benzene. *Inorg. Chem.* **2007**, *46*, 1992–2001.
- (50) Harkins, S. B.; Peters, J. C. A Highly Emissive Cu₂N₂ Diamond Core Complex Supported by a [PNP][−] Ligand. *J. Am. Chem. Soc.* **2005**, *127*, 2030–2031.
- (51) McMillin, D. R.; McNett, K. M. Photoprocesses of Copper Complexes That Bind to DNA. *Chem. Rev.* **1998**, *98*, 1201–1220.
- (52) Blasse, G.; McMillin, D. R. On the Luminescence of Bis (Triphenylphosphine) Phenanthroline Copper (I). *Chem. Phys. Lett.* **1980**, *70*, 1–3.
- (53) Araki, H.; Tsuge, K.; Sasaki, Y.; Ishizaka, S.; Kitamura, N. Luminescence Ranging from Red to Blue: A Series of Copper(I)–Halide Complexes Having Rhombic {Cu₂(M-X)₂} (X = Br and I) Units with N-Heteroaromatic Ligands. *Inorg. Chem.* **2005**, *44*, 9667–9675.
- (54) Okano, Y.; Ohara, H.; Kobayashi, A.; Yoshida, M.; Kato, M. Systematic Introduction of Aromatic Rings to Diphosphine Ligands for Emission Color Tuning of Dinuclear Copper(I) Iodide Complexes. *Inorg. Chem.* **2016**, *55*, 5227–5236.
- (55) Chai, W.; Hong, M.; Song, L.; Jia, G.; Shi, H.; Guo, J.; Shu, K.; Guo, B.; Zhang, Y.; You, W.; Chen, X. Three Reversible Polymorphic Copper(I) Complexes Triggered by Ligand Conformation: Insights into Polymorphic Crystal Habit and Luminescent Properties. *Inorg. Chem.* **2015**, *54*, 4200–4207.
- (56) Cunningham, C. T.; Cunningham, K. L. H.; Michalec, J. F.; McMillin, D. R. Cooperative Substituent Effects on the Excited States of Copper Phenanthrolines. *Inorg. Chem.* **1999**, *38*, 4388–4392.
- (57) Ohara, H.; Kobayashi, A.; Kato, M. Simple and Extremely Efficient Blue Emitters Based on Mononuclear Cu(I)-Halide Complexes with Delayed Fluorescence. *Dalton Trans.* **2014**, *43*, 17317–17323.
- (58) Kaeser, A.; Mohankumar, M.; Mohanraj, J.; Monti, F.; Holler, M.; Cid, J.-J.; Moudam, O.; Nierengarten, I.; Karmazin-Brelot, L.; Duhayon, C.; Delavaux-Nicot, B.; Armaroli, N.; Nierengarten, J.-F. Heteroleptic Copper(I) Complexes Prepared from Phenanthroline and Bis-Phosphine Ligands. *Inorg. Chem.* **2013**, *52*, 12140–12151.
- (59) Ohara, H.; Kobayashi, A.; Kato, M. Effects of N-Heteroaromatic Ligands on Highly Luminescent Mononuclear Copper(I)–Halide Complexes. *C. R. Chim.* **2015**, *18*, 766–775.
- (60) Filonenko, G. A.; Fayzullin, R. R.; Khusnutdinova, J. R. Intramolecular Non-Covalent Interactions as a Strategy Towards Controlled Photoluminescence in Copper(I) Complexes. *J. Mater. Chem. C* **2017**, *5*, 1638–1645.
- (61) Khusnutdinova, J. R.; Luo, J.; Rath, N. P.; Mirica, L. M. Late First-Row Transition Metal Complexes of a Tetradentate Pyridinophane Ligand: Electronic Properties and Reactivity Implications. *Inorg. Chem.* **2013**, *52*, 3920–3932.
- (62) Meneghetti, S. P.; Lutz, P. J.; Kress, J. Neutral and Cationic Palladium(II) Complexes of a Diazapyridinophane. Structure, Fluxionality, and Reactivity toward Ethylene. *Organometallics* **2001**, *20*, 5050–5055.
- (63) Khusnutdinova, J. R.; Rath, N. P.; Mirica, L. M. The Conformational Flexibility of the Tetradentate Ligand ^{tBu}N₄ is Essential for the Stabilization of (^{tBu}N₄)Pd^{III} Complexes. *Inorg. Chem.* **2014**, *53*, 13112–13129.
- (64) Chen, L. X.; Shaw, G. B.; Novozhilova, I.; Liu, T.; Jennings, G.; Attenkofer, K.; Meyer, G. J.; Coppens, P. MLCT State Structure and Dynamics of a Copper(I) Diimine Complex Characterized by Pump-Probe X-Ray and Laser Spectroscopies and DFT Calculations. *J. Am. Chem. Soc.* **2003**, *125*, 7022–7034.
- (65) Chen, L. X.; Jennings, G.; Liu, T.; Gosztola, D. J.; Hessler, J. P.; Scaltrito, D. V.; Meyer, G. J. Rapid Excited-State Structural Reorganization Captured by Pulsed X-Rays. *J. Am. Chem. Soc.* **2002**, *124*, 10861–10867.
- (66) Filonenko, G. A.; Khusnutdinova, J. R. Dynamic Phosphorescent Probe for Facile and Reversible Stress Sensing. *Adv. Mater.* **2017**, *29*, 1700563–1700568.
- (67) Tang, F.; Qu, F.; Khusnutdinova, J. R.; Rath, N. P.; Mirica, L. M. Structural and Reactivity Comparison of Analogous Organometallic Pd(III) and Pd(IV) Complexes. *Dalton Trans* **2012**, *41*, 14046–14050.
- (68) Bottino, F.; Di Grazia, M.; Finocchiaro, P.; Fronczek, F. R.; Mamo, A.; Pappalardo, S. Reaction of Tosylamide Monosodium Salt with Bis(Halomethyl) Compounds: An Easy Entry to Symmetrical N-Tosyl Aza Macrocycles. *J. Org. Chem.* **1988**, *53*, 3521–3529.
- (69) Kubas, G. J.; Monzyk, B.; Crumblis, A. L. *Inorganic Synthesis*; John Wiley & Sons, Inc.: New York, 2007.
- (70) Jarek, R. L.; Flesher, R. J.; Shin, S. K. Kinetics of Internal Rotation of N,N-Dimethylacetamide; a Spin-Saturation Transfer Experiment. An Undergraduate Physical Chemistry Experiment Using FT-NMR to Determine an Internal Rotational Barrier. *J. Chem. Educ.* **1997**, *74*, 978–982.
- (71) See the [Supporting Information](#).
- (72) Farrugia, L. J. WinGX and ORTEP for Windows: An Update. *J. Appl. Crystallogr.* **2012**, *45*, 849–854.
- (73) Sheldrick, G. ShelXT - Integrated Space-Group and Crystal-Structure Determination. *Acta Crystallogr., Sect. A: Found. Adv.* **2015**, *71*, 3–8.
- (74) Sheldrick, G. Crystal Structure Refinement with ShelXL. *Acta Crystallogr., Sect. C: Struct. Chem.* **2015**, *71*, 3–8.
- (75) Flack, H. D.; Bernardinelli, G. Reporting and Evaluating Absolute-Structure and Absolute-Configuration Determinations. *J. Appl. Crystallogr.* **2000**, *33*, 1143–1148.
- (76) Kühn, U.; Warzeska, S.; Pritzkow, H.; Krämer, R. A Bioinspired Dicopper(II) Catalyst for the Transesterification of Dimethyl Phosphate. *J. Am. Chem. Soc.* **2001**, *123*, 8125–8126.
- (77) Jagoda, M.; Warzeska, S.; Pritzkow, H.; Wadepohl, H.; Imhof, P.; Smith, J. C.; Krämer, R. Catalytic Transesterification of Dialkyl Phosphates by a Bioinspired Dicopper(II) Macrocyclic Complex. *J. Am. Chem. Soc.* **2005**, *127*, 15061–15070.
- (78) Warzeska, S.; Kramer, R. A Dicopper (II) Complex of a New Octaaza Macrocyclic: A Receptor in the Entatic State. *Chem. Commun.* **1996**, 499–500.
- (79) Prince, E. Mathematical, Physical and Chemical Tables. *International Tables for Crystallography*, 3rd ed.; Kluwer Academic Publishers: Dordrecht, The Netherlands, 2004; Vol. C.
- (80) Addison, A. W.; Rao, T. N.; Reedijk, J.; van Rijn, J.; Verschoor, G. C. Synthesis, Structure, and Spectroscopic Properties of Copper(II) Compounds Containing Nitrogen-Sulphur Donor Ligands; the Crystal and Molecular Structure of Aqua[1,7-Bis(N-Methylbenzimidazol-2'-yl)-2,6-Dithiaheptane]Copper(II) Perchlorate. *J. Chem. Soc., Dalton Trans.* **1984**, 1349–1356.
- (81) Yang, L.; Powell, D. R.; Houser, R. P. Structural Variation in Copper(I) Complexes with Pyridylmethylamide Ligands: Structural Analysis with a New Four-Coordinate Geometry Index, τ_4 . *Dalton Trans.* **2007**, 955–964.
- (82) Okuniewski, A.; Rosiak, D.; Chojnacki, J.; Becker, B. Coordination Polymers and Molecular Structures among Complexes

of Mercury(II) Halides with Selected 1-Benzoylthioureas. *Polyhedron* **2015**, *90*, 47–57.

(83) The crystals were obtained by the slow diffusion of diethyl ether vapors into a dichloromethane solution; the crystalline product was analyzed by XRD, and the structure (1833073) was submitted to CCDC.

(84) All spectra were recorded using 600 MHz NMR spectrometer. Because of the larger chemical shift difference between meta protons in other complexes, such a comparison cannot be made directly.

(85) A similar treatment was not possible for complex **5** because three-site exchange occurs under these conditions, including degenerative exchange in the tetracoordinate complex and formation of a pentacoordinate isomer. For complex **7**, selective signal irradiation could not be achieved because of the close spacing between aromatic peaks.

(86) Zanello, P.; Nervi, C.; Fabrizi de Biani, F. *Inorganic Electrochemistry: Theory, Practice and Application*, 2nd ed.; Royal Society of Chemistry: London, 2012.

(87) Zink, D. M.; Volz, D.; Baumann, T.; Mydlak, M.; Flügge, H.; Friedrichs, J.; Nieger, M.; Bräse, S. Heteroleptic, Dinuclear Copper(I) Complexes for Application in Organic Light-Emitting Diodes. *Chem. Mater.* **2013**, *25*, 4471–4486.

(88) The emission spectra of complexes **A**, **5**, and **8** in THF show a hypsochromic shift at 77 K compared to the spectra at 298 K, which is not consistent with TADF (e.g., see: Nitsch, J.; et al. *Chem. Commun.* **2016**, *52*, 2932–2935).

(89) Williford, C. J.; Stevens, E. P. Strain Energies as a Steric Descriptor in QSAR Calculations. *QSAR Comb. Sci.* **2004**, *23*, 495–505.

(90) Eliel, E. L.; Wilen, S. H.; Mander, L. N. *Stereochemistry of Organic Compounds*; John Wiley & Sons: New York, 1994.

(91) Anslyn, E. V.; Dougherty, D. A.; Dougherty, E. V. *Modern Physical Organic Chemistry*; University Science Books: Herndon, VA, 2006.

(92) In particular, the correlation is observed with the AG_{60} steric parameter based on the different stabilities of gauche and anti conformers of substituted propanes, described in ref **89**, and A values (see refs **89–91**).

(93) Felder, D.; Nierengarten, J.-F.; Barigelletti, F.; Ventura, B.; Armaroli, N. Highly Luminescent Cu(I)–Phenanthroline Complexes in Rigid Matrix and Temperature Dependence of the Photophysical Properties. *J. Am. Chem. Soc.* **2001**, *123*, 6291–6299.

(94) Cunningham, C. T.; Moore, J. J.; Cunningham, K. L. H.; Fanwick, P. E.; McMillin, D. R. Structural and Photophysical Studies of $\text{Cu}(\text{NN})_2^+$ Systems in the Solid State. Emission at Last from Complexes with Simple 1,10-Phenanthroline Ligands. *Inorg. Chem.* **2000**, *39*, 3638–3644.

(95) Cuttall, D. G.; Kuang, S.-M.; Fanwick, P. E.; McMillin, D. R.; Walton, R. A. Simple Cu(I) Complexes with Unprecedented Excited-State Lifetimes. *J. Am. Chem. Soc.* **2002**, *124*, 6–7.

(96) Everly, R. M.; Ziessel, R.; Suffert, J.; McMillin, D. R. Steric Influences on the Photoluminescence from Copper(I) Phenanthrolines in Rigid Media. *Inorg. Chem.* **1991**, *30*, 559–561.